Research Square

Preprints are preliminary reports that have not undergone peer review.
They should not be considered conclusive, used to inform clinical practice,
or referenced by the media as validated information.

Time-varying gene expression network analysis for evolution of human prefrontal cortex

Yuehua Cui (cuiy@msu.edu)
Michigan State University https://orcid.org/0000-0001-8099-1753
Huihui Wang
Shanxi Medical University
Yongqing Wu
Shanxi Medical University
Jian Sa
Shanxi Medical University
Zhi Li
Shanxi Medical University
Hongyan Cao
Shanxi Medical University

Research article

Keywords: Human PFC; Gene network evolution; Time-varying graph; loggle model; Hub gene

Posted Date: May 11th, 2020

DOI: https://doi.org/10.21203/rs.3.rs-26819/v1

License: This work is licensed under a Creative Commons Attribution 4.0 International License.
Read Full License

Time-varying gene expression network analysis for evolution of the human prefrontal cortex

Huihui Wang[1], Yongqing Wu[1], Jian Sa[1], Zhi Li[2], Hongyan Cao[1,*], and Yuehua Cui[3,*]

[1]*Division of Health Statistics, School of Public Health, Shanxi Medical University, Taiyuan, Shanxi 030001, PR China*

[2]*School of Sport and Physical Education, North University of China, Taiyuan, Shanxi 030051, PR China*

[3]*Department of Statistics and Probability, Michigan State University, East Lansing, MI 48824, USA*

Running head: Time-varying network analysis

*Corresponding authors: Hongyan Cao (cao_hong_yan@163.com) and Yuehua Cui (cuiy@msu.edu)

Abstract

Background: The prefrontal cortex (PFC) constitutes a large part of the human central nervous system and is essential for the normal social affection and executive function of humans and other primates. Despite ongoing research in this region, the evolution of interactions between PFC genes is still unknown, and there is a need to better understand changes in expression of age-related genes over the lifespan. To investigate the evolution of PFC gene interaction networks and further identify hub genes, we obtained time-series gene expression data of human PFC tissues from the Gene Expression Omnibus (GEO) database. A statistical model, loggle, was used to construct time-varying networks and explore the evolution of PFC gene networks over time. Several common network attributes were used to explore the evolution of PFC gene networks over time. The hub genes of different evolutionary stages were identified. At the same time, we explored several known KEGG pathways in PFC and the corresponding development patterns of central genes.

Results: Network similarity analysis showed that the development of human PFC is divided into three stages, namely, fast development period, deceleration to stationary period, and destructive recession period. We identified some genes related to PFC evolution at these different stages, including genes involved in neuronal differentiation or synapse formation, genes involved in nerve impulse transmission, and genes involved in the development of myelin around neurons. Some of these genes are consistent with findings in previous reports. Pathway evolution analysis suggests that the axon guidance pathway has been most responsive during the evolution of PFC.

Conclusions: This study clarified the evolutionary trajectory of the interaction between PFC genes, and proposed a set of candidate genes related to PFC development, which helps further study of human brain development at the genomic level supplemental to regular anatomical analyses. The analytical process used in this study, involving the loggle model, similarity analysis, and central analysis, provides a comprehensive strategy to gain novel insights into the evolution and development of brain networks in other organisms.

Keywords: Human PFC; Gene network evolution; Time-varying graph; loggle model; Hub gene

Background

The prefrontal cortex (PFC), covering the front part of the frontal lobe, receives input from multiple regions of the brain for information processing [1, 2], and is a key area for studying the evolution and mechanisms of decline of the human brain. It plays important roles in emotional and social behavior, coordinating complex cognitive behavior, expression, and decision-making [3, 4]. PFC development is greatly shaped by gene expression, which is dynamically regulated across a person's lifespan [5]. By mapping the key features of the evolutionary trajectory of PFC gene expression, not only can the dynamic development of brain function be revealed, but also our understanding of the mechanisms that drive cellular responses can be promoted [6, 7].

Since it is obviously impossible to perform biopsies from the same area of an individual's brain multiple times during growth to generate time-series genetic data, in the past few decades, researchers have evaluated the developmental trajectory of the forehead from the perspectives of neuropsychology, neuroimaging, and cell physiology [8-11]. It is generally believed that the neuro-physiological development of the forehead experiences a pattern of first increasing and then decreasing to a steady state (cubic). For example, Shaw and colleagues simulated the changes in the cerebral cortex by combining longitudinal neuroanatomical imaging data with cross-sectional data. They found that the developmental trajectory of the frontal cortex was cubic, that is, it increases first and then gradually decreases to a steady state [6]. With the advancement of science and technology, researchers have constructed time-series genetic data from a single biopsy of multiple individuals and characterized similar developmental trajectories at the genetic level, but only explored this based on the expression level of individual genes [12, 13]. For example, Xiling et al. [14] used unsupervised hierarchical clustering to cluster the PFC genes and found that the expression levels of genes related to neuronal activity show a trend of rising then decreasing throughout the lifespan. Although previous studies clearly observed age-related changes in PFC development from the anatomical structure and individual gene expression levels, the generation of cell diversity during human brain development requires precise regulation between genes [15, 16]. The temporal dynamics of this intergenic interaction is yet to be delineated.

As a statistical tool, network analysis can help us obtain a holistic understanding of complex systems, rather than just the individual nodes of which they consist [17]. However, network graphs created with time-varying data may also change over time. It is biologically meaningful to study the evolution of these graphs over time rather than characterizing one single graph [18, 19]. To cope with the challenge of time-series data, some methods have been developed using the Gaussian Graphic Model (GGM) [20] to estimate time-varying graphs [21-24] while assuming that the covariance matrices change smoothly over time; this facilitates understanding and explanation of the interaction of network nodes [19]. Yang and Peng proposed the Local Group Graphical Lasso Estimation (loggle) [19] model based on the assumption that the graph topology changes gradually over time to estimate the inverse covariance matrix to construct the edge sets. This method effectively utilizes neighborhood information, and saves computational time by using a blockwise fast algorithm and pseudo-likelihood approximation. The successful application of the loggle model in the work of Yang and Peng [19] illustrates how direct interactions between stocks evolved over time under the influence of the global financial crisis.

In this work, we apply the loggle model to a time-series gene expression data set to construct PFC time-varying gene interaction networks, since the model fits the biological realm of PFC development and evolution. We quantify the evolutionary trend of the PFC gene network through network global attribute indicators such as network diameter. We further apply network similarity analysis to describe the evolutionary stage of PFC, so as to identify hub genes at different stages using the central analysis. We also apply the loggle model to evaluate the evolution of several KEGG pathways in PFC. The identification of the evolutionary changes of gene networks in human PFC can provide novel insights into human brain development and function. The hub genes identified in different evolutionary stages provide specific candidate targets for further biological validation.

Results

Data

Human PFC time-series gene expression data

The time-series gene expression data on the human PFC were downloaded from the GEO database (http://www.ncbi.nlm.nih.gov/geo) with Gene Expression Omnibus accession number GSE30272. This data set records 269 RNA samples from stages from fetus development to elderly (14 gestational weeks to 80 years). Subjects with severe neurological or psychiatric conditions were excluded. These samples were obtained from postmortem human brain PFC gray matter tissue homogenates and subjected to a series of processes such as RNA extraction and quality control. The log2 intensity ratio was normalized after background correction, and the log2 ratio was further adjusted to reduce the impact of system noise after performing surrogate variable analysis. Readers are referred to the paper by Colantuoni et al. [62] for a detailed description of the data source and processing procedures. After probe annotation and data cleaning, a time-series gene expression matrix of 17,150×269 was generated for further statistical analysis.

Initial feature selection

Considering data noise and the complexity of the algorithms that would be used to construct a time-varying graph, we first performed feature screening to filter out potential noise and reduce the data dimensionality. In this work, we considered the following two options for feature screening to obtain genes that carry important information.

(i) Calculate the variance for each gene and select the top 300 genes to construct the time-varying network graphs. Genes with smaller variance do not show much variation across the time domain and thus are not considered. The purpose of this is to explore the evolution of networks constructed with genes showing high variation in PFC throughout the lifespan.

(ii) Select genes based on known KEGG pathways. The purpose of this is to explore the evolution of several known pathways of PFC throughout the lifespan. In this study, we chose five pathways related to PFC function by searching the literature. A list of the pathways is shown in Table 1, together with the pathway entry and name, the number of genes in the pathway, and the number of genes mapped to the pathway in this data set. A total of five systems related to PFC or sensitive to age changes are involved, namely, signal transduction (hsa04068), immune system

(hsa04611), nervous system (hsa04728), aging (hsa04211), and development and regeneration (hsa04360), to understand the developmental trends of these pathways in the PFC area over time.

Table 1. Selected pathway information

Pathway entry	Pathway name	# of genes in the pathway	# of genes mapped to the pathway
hsa04728	*Dopaminergic synapse pathway*	131	123
hsa04211	*Longevity regulating pathway*	89	80
hsa04360	*Axon guidance pathway*	181	171
hsa04611	*Platelet activation pathway*	124	110
hsa04068	*FoxO signaling pathway*	131	118

Age grouping

We built the time-varying network by dividing the sample into nine age periods based on the age information provided by the original data [62], that is, fetus (14–20 gestational weeks), infant (0–6 months), child (1–10 years), 10s (10–20 years), 20s (20–30 years), 30s (30–40 years), 40s (40–50 years), 50s (50–60 years), and 60s (60 years or older).

Comparisons of loggle, kernel, and invar

A gene expression heatmap was drawn to show the age distribution of the data and provide a reference for model comparison (Fig. 1). A quick look at Fig. 1 reveals that PFC gene expression fluctuates significantly throughout the lifespan, with very low or high expression from the fetus to infant period, and then gradually stabilizes after the child stage. The expression of a large number of genes is highly disturbed (up- or downregulated) at an early stage; then, this number gradually decreases in later stages.

Table 2 shows the cross-validation results of the three models. We can see that loggle has a smaller CV score than kernel and invar. In addition, loggle and kernel have fewer average edges, while invar has more edges. Furthermore, from Fig. 2, we can see that the PFC time-varying graph constructed by the invar model does not change throughout the lifespan. In contrast, the PFC time-varying graph constructed by the loggle and kernel models captures the evolving pattern over time. The network structure is more complex (e.g., has more edges) during the early stage and then

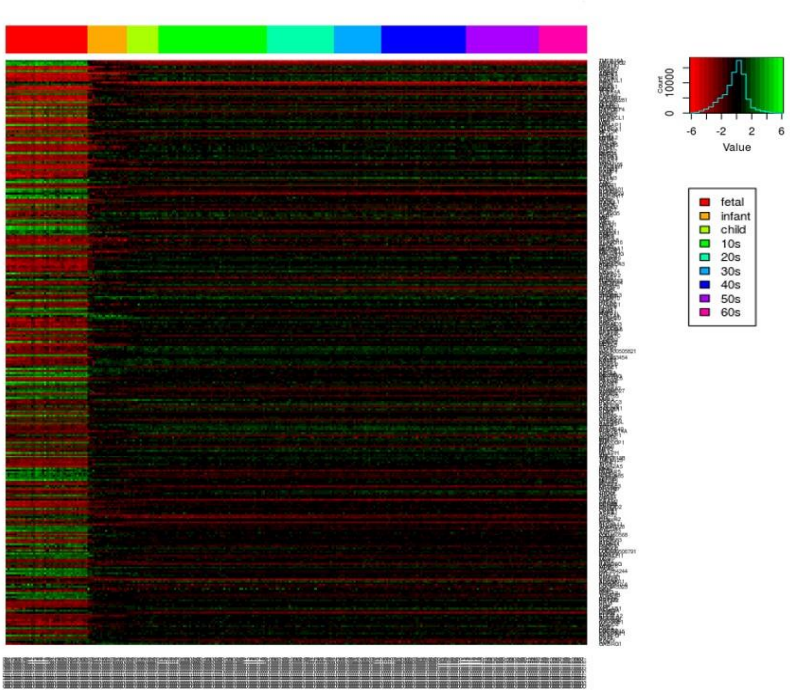


Fig. 1 PFC global gene expression changes over time. Each row of the heatmap represents a gene, and each column represents a sample. Each small grid represents the expression of a gene in the sample, with red representing relatively low expression and green high expression. Different colored bars at the top of the graph indicate the age group to which the sample belongs, as shown in the legend on the right.

gradually falls into a stationary state, which is consistent with the human prefrontal cortex development pattern and is similar to the previous heatmap results. Thus, both the loggle and the kernel models can describe the evolutionary mode of PFC well, but the loggle model has a better CV score and is better supported by data. Finally, we chose the well-balanced loggle model for further analysis. Table S1 in the Supplemental File shows the result of the parameter selection of the loggle model at each age stage.

Table 2. List of average # of edges and cv.score using different method.

Method	Average # of edge	cv.score
loggle	224.2	-309.64
kernel	139.0	Inf
invar	442.0	Inf

Evolution of human PFC time-varying network graph

Based on the above model comparison results, we selected the best performing loggle model results to further analyze the evolution of the human brain PFC tissue gene expression network over time. The time-varying graph of the gene interaction network fitted by this model is shown in Fig. 3. For the list of edges corresponding to each age group network, please refer to the

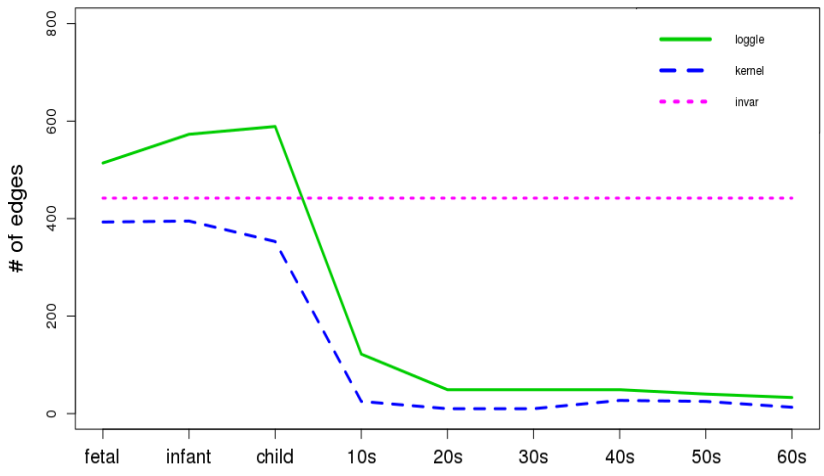


Fig. 2 Number of edges vs. age period (x-axis). Different line types represent different models.

supplementary materials. The trends of change of the number of nodes and the number of edges of the corresponding network are shown in Fig. 4A. It is observed that, from the fetus stage to the child stage, with increasing age, the complexity of the PFC gene interaction network begins to increase gradually, peaking in the child stage. During this time, the number of edges of the network is also much higher than the number of nodes (see Fig. 4A). Compared with the case at older ages, the inner edge of the network is more complicated. This demonstrates that most of the genes in the PFC region are very active during this time period, in which rapid development occurs. After that, the number of edges decreases rapidly between 10 and 20 years old (child stage to the 10s), and the number of active nodes also decreases. This shows that the development rate of PFC gradually slows down. After the 10s, the numbers of edges and nodes gradually plateau, and the edge composition inside the network is simplified. This indicates that the development speed gradually decreases. It tends to be stable after the 20s. Moreover, after the 50s, it breaks the stability and

shows a downward trend again. Thus, the PFC time-varying network model presents a cubic, with rapid development in early life, a trend of moderate growth in middle age, and then a slight decline later in life. This proves the continuous long-term changes of the PFC gene expression network, echoing the findings of a previous report [26].

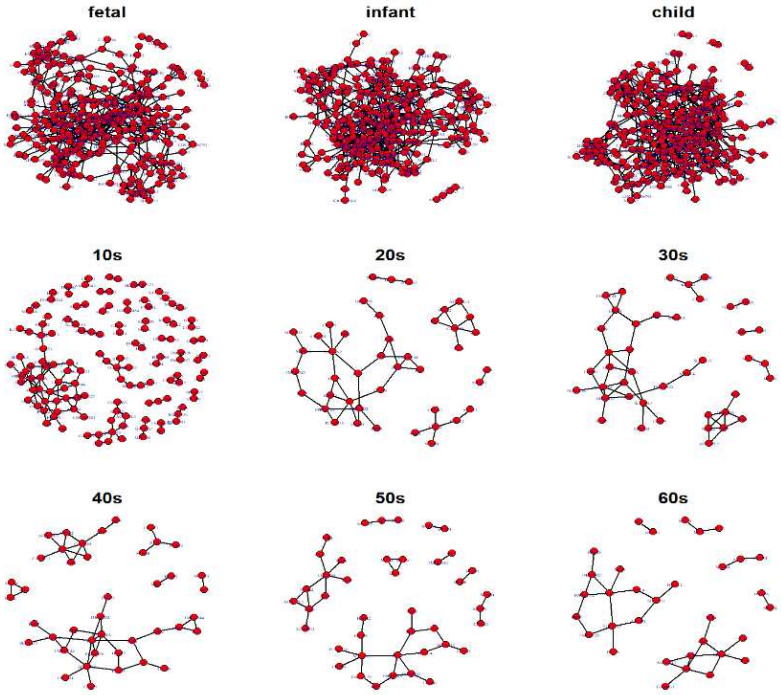


Fig. 3 Display of networks corresponding to the nine age periods. Nodes represent genes and connections between nodes indicate interactions between genes.

To illustrate the changes in the network topology in more detail, we calculated several global network properties. As seen in Fig. 4B, in the early stage of life (fetus to the 10s), the network diameter is large and the network density is low. After that, the network diameter gradually decreases. Interestingly, the network density then gradually increases in the 10s, although there are slight fluctuations. This implies that the time-varying network graph of PFC is relatively sparse in early life and gradually becomes denser with aging. In addition, compared with the late period, there are more exclusive edges in the first four stages of life, and the number of exclusive edges in the child period is the highest, which further indicates that this is a period of rapid development of human PFC. During this period, some unique biological processes occur to promote the development of PFC.

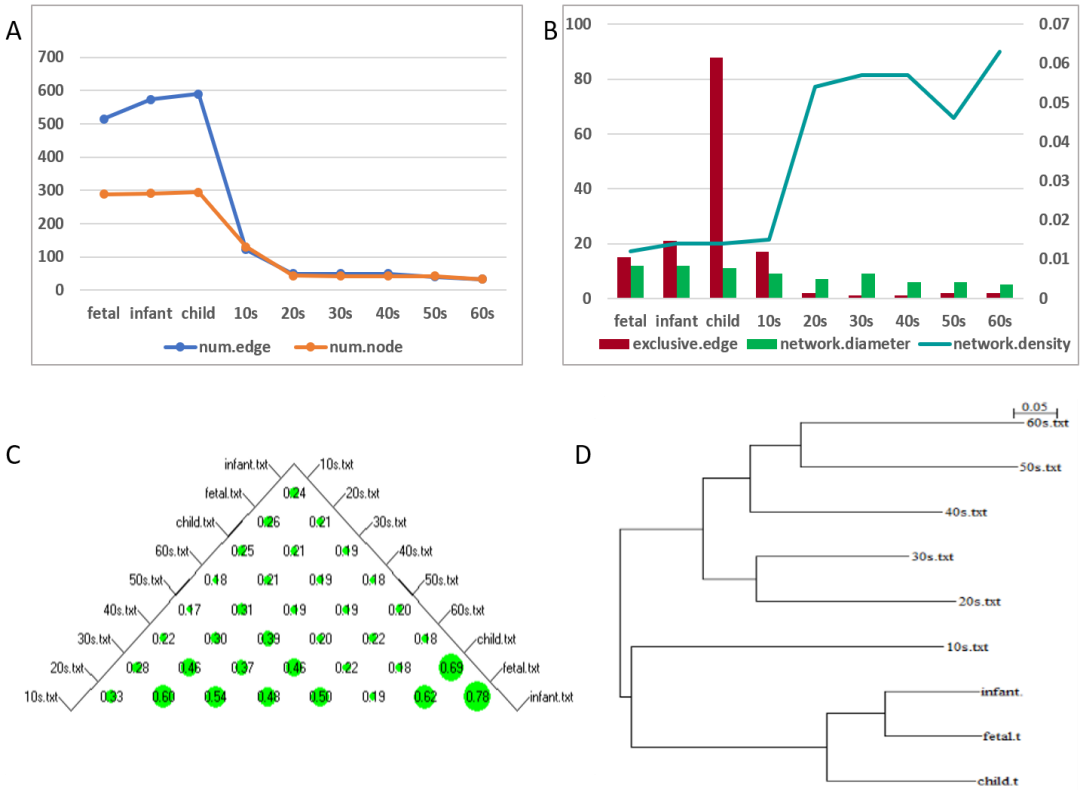


Fig. 4 Network topology change. (A) shows the numbers of edges and nodes included in the network at different ages. (B) represents the specific edge (left y-axis), network diameter (left y-axis), and network density (right y-axis) in the network corresponding to each age period. (C) shows a bubble chart of a similarity matrix generated based on the CNSI. Larger bubbles indicate higher similarity of the corresponding two networks. (D) is a hierarchical clustering tree dendrogram generated based on the similarity matrix.

We further analyzed the similarity between the networks of the nine age periods using the CNSI indicator (see methods for details). As shown in Fig. 4C, the similarity between the networks corresponding to the two periods of fetus and infant is the highest (0.78), followed by infant and child (0.69). The corresponding hierarchical clustering tree (Fig. 4D) aggregates these three periods into one category. A closer look at this bubble chart also reveals that the similarity between the 20s and the 30s is also very high (0.6), and the tree diagram puts them in the same cluster. The similarity among the 40s, 50s, and 60s is also high, and their distances in the tree are also short. In contrast, the similarity between the 10s and other networks is low, and the dendrogram places 10s in separate clusters.

Based on these results, we divided the evolution of PFC into three stages, namely, fast development period (fetus, infant, child), deceleration to stationary period (10s, 20s, 30s), and destructive recession period (40s, 50s, 60s). Central analysis was performed separately to identify

hub genes at these three different stages.

Hub genes accompanying the evolution of human PFC

To explore important genes involved in the evolution of the human PFC gene interaction network throughout the lifespan, we calculated the node *degree* of the network graph at each time point. According to the above evolutionary analysis of the network, three developmental stages were considered to identify hub genes (Fig. 5). From Fig. 5A, we can see that the hub genes in the fast development period of PFC evolution are as follows: *STK32B*, *CX3CL1*, and *BACH2* in the fetus stage; *STK32B*, *PCSK1*, and *NPPA* in infant; and *IPCEF1*, *STK32B*, and *RGS4* in child. The hub genes in the deceleration to stationary period of PFC evolution (Fig. 5B) are as follows: *EVI2A* and *TF* in the 10s, *SLC31A2* and *TF* in the 20s, and *GJB6* and *TF* in the 30s. Finally, the hub genes in the destructive recession period of PFC evolution (Fig. 5C) are as follows: *SLC31A2*, *GJB6*, and *PLLP* in the 40s; *SLC31A2*, *CLDN10*, and *PLLP* in the 50s; and *CLDN10*, *GJB6*, and *PLLP* in the 60s. Interestingly, we found that some genes are consistently identified as hub genes at different age periods within the same stage. For example, the gene *STK32B* is consistently identified as a hub gene at the three age periods during the fast development stage, the gene *TF* functions consistently as a hub gene in the deceleration to stationary period, and the same applies for the gene *PLLP* in the destructive recession period. This indicates the importance of these genes in the evolution of the human PFC gene network. The biological functions associated with most of them provide further detailed information for discovering biological functions involved in PFC development with age.

Evolution of five known pathways in PFC and the identification of hub genes

Here, we selected five pathways related to brain function (see Table 2 for details) to see the developmental trend in PFC over time. The parameter selection results by loggle are shown in Table S2 in the Supplemental File. Using the parameters, we constructed network graphs and the network evolution trends are shown in Fig. 6.

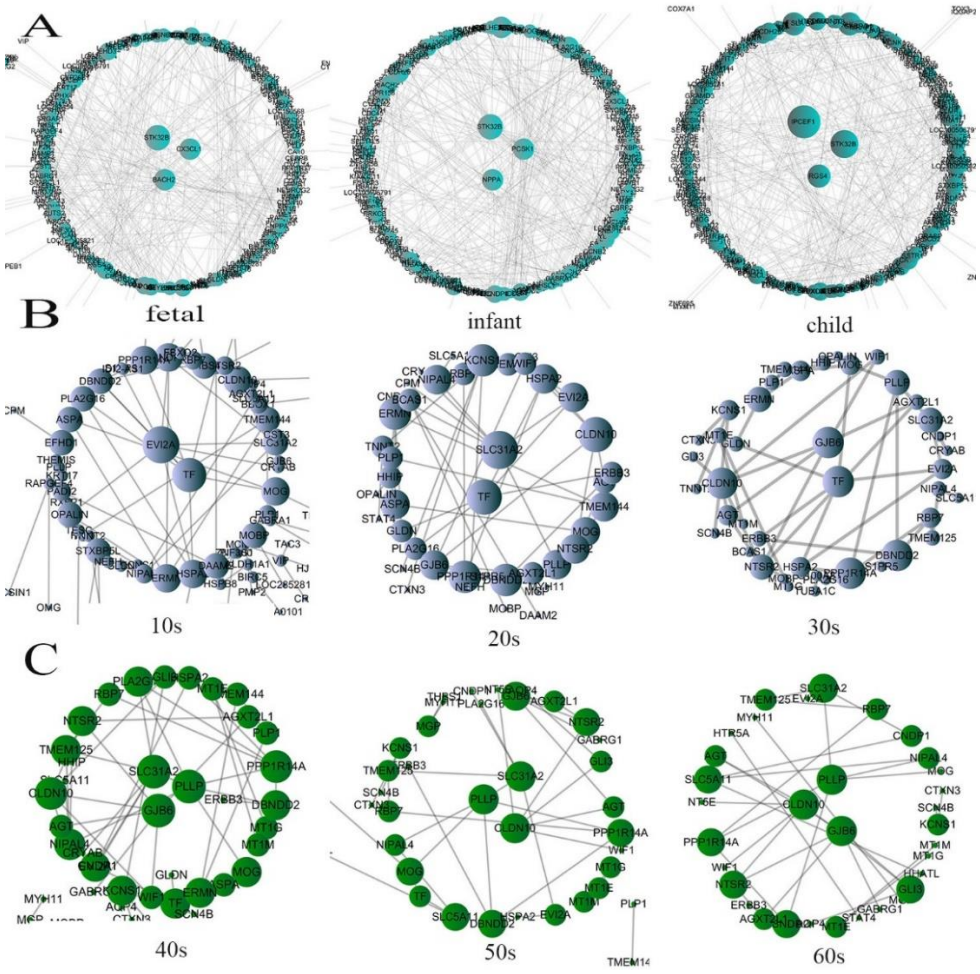


Fig. 5 Identification of hub genes throughout the lifespan in PFC evolution. (A) shows the fast development period of PFC evolution, namely, fetus, infant, and child; (B) shows that the evolution of PFC gradually declined to a stable period, that is, 10s, 20s, and 30s; (C) demonstrates the destructive recession period in PFC evolution, namely, 40s, 50s, and 60s. A larger node size in the graph corresponds to a higher node degree. Nodes with the highest degree are considered to be hubs and are placed in the network center.

From Fig. 6 we can see that, as age increases, the number of network edges in these five pathways gradually decreases. From the fetus to the child stage, the network size of these pathways remains largely stable, meaning that most genes involved in these pathways are mostly active in the PFC region during this time period. Then, from the child stage to the 30s, the numbers of edges and genes in all pathways gradually decrease; thus, development gradually slows down and eventually remains relatively stable after the 30s. Among the pathways, the pathway hsa04360 (*Axon guidance pathway*) has the most nodes and edges, with the fastest change from child to 30s. Among the five pathways, the *Axon guidance pathway* is most sensitive to age changes, followed

by three pathways: the *Dopaminergic synapse pathway* (hsa04728), the *Platelet activation pathway* (hsa04611), and the *FoxO signaling pathway* (hsa04068). These three pathways not only have similar numbers of nodes and edges in PFC, but also the rates of change in the declining period are similar, and the numbers of edges in the stationary period are also similar. In contrast, the *Longevity regulating pathway* (hsa04211) has the fewest nodes and edges, the slowest rate of change in the declining period, and the lowest number of edges in the final stationary stage. The results provide evidence that these pathways are highly active during the fast development stage and are abolished with the slowing down of PFC development.

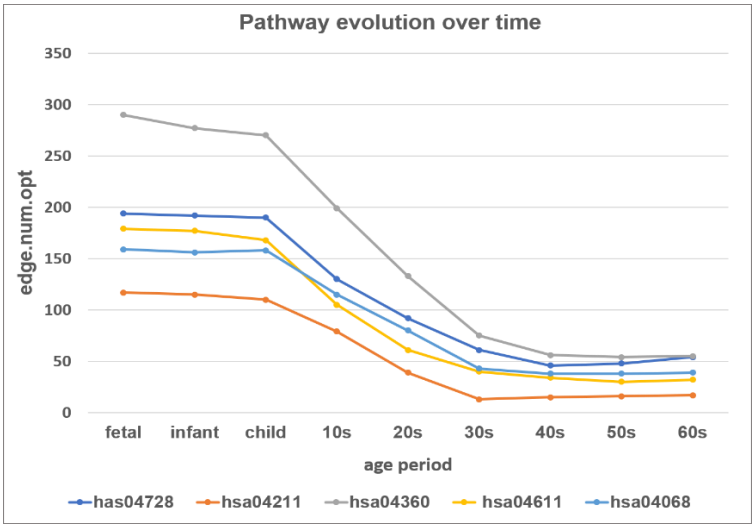


Fig. 6 The evolution of the time-varying networks over different age periods. The y-axis shows the optimal number of edges at each developmental stage.

We further explored the hub genes of these pathways at the fast development period (fetus, infant, and child), as shown in Fig. 7. We found that the hub genes of each pathway during this period are nearly unchanged. Among them, the hub genes for the *Dopaminergic synapse pathway* (hsa04728) are *PRKCB* and *GNG7*; for the *Longevity regulating pathway* (hsa04211) are *IGF1* and *PRKAB2*; for the *Axon guidance pathway* (hsa04360) are *LRRC4C* and *PARD6G*; for the *Platelet activation pathway* (hsa04611) are *TLN2* and *RASGRP2*; and for the *FoxO signaling pathway* (hsa04068) are *CCNB1* and *PRKAB2*, while one additional gene *SMAD3* is shown in the child stage.

We also performed a central analysis of the other two developmental stages, the declining stage (10s, 20s, and 30s) and the stable stage (40s, 50s, and 60s). Owing to limits of space, we placed

241 the results in the Supplemental File. Please see Fig. S1 and S2 for more details.

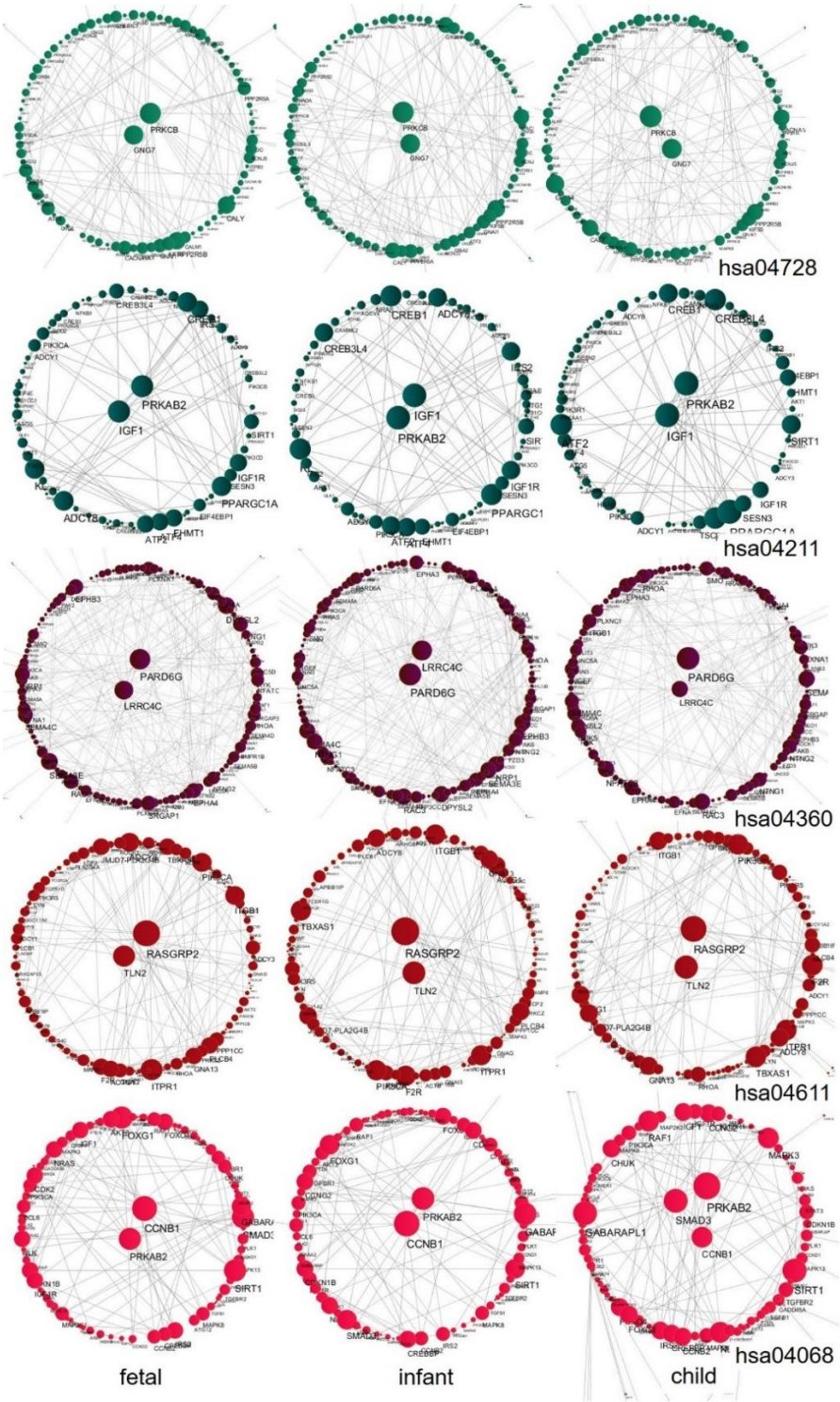


Fig. 7 Central analysis of networks corresponding to the fast development stage (fetus, infant, and child) for the five pathways. A larger node corresponds to a larger node degree. Hub genes with large node degree values in each network are placed in the center of the network.

242

Discussion

In this work, we proposed a comprehensive network analysis strategy, which was demonstrated based on the time-series gene expression data of human PFC tissue. The loggle model was used to reconstruct the evolutionary trajectory of the time-varying network graph of gene interaction, not at the level of gene expression. At the same time, the evolution of PFC was divided into three stages by similarity analysis, and hub genes at different developmental stages were identified. In addition, several known KEGG pathways related to brain function were chosen for analysis to further demonstrate the analytical procedure.

The evolution of time-varying graphs reveals the developmental pattern of human PFC

Owing to its functional properties, development of the human brain usually continues for a long time, starting with the fetus and continuing through adolescence. PFC is one of the last brain regions to mature [25]. Studies have demonstrated from histological and cognitive perspectives that the developmental characteristics of PFC exhibit rapid development in early childhood, decelerate in adolescence, and then gradually reach a mature and stable state in adulthood [26], after which a change to a destructive manner occurs in old age [27].

Although the macro-level PFC evolution model has been widely accepted, owing to technological limitations, the trend of evolution at the gene interaction level has not been clearly described. To fill this gap, in our study, we used time-series gene expression data to construct the evolutionary pattern of PFC at the molecular level by estimating the time-varying network graphs. We found that, from the fetus to child stages, PFC experiences fast development and most genes are active during this period. A review by Teffer et al. [26] described that, as the brain size increases and changes in microstructures such as synapses occur throughout childhood, the number of neurons in the entire cortex increases. The density of neurons in the frontal lobe does not peak until later childhood. According to Anderson [28], the fast development of logical reasoning capabilities that rely on cognitive functions also occurs between the ages of 6 and 9. After that, the development speed drops dramatically. This period is accompanied by a decrease in the volume of gray matter, a corresponding increase in the volume of white matter, and a decrease in synaptic

density [29]. After the age of 20, it tends to be stable, and its development is basically maintained at a low level. After the age of 50, a destructive decline occurs. Unsurprisingly, the trend of PFC evolution coincides with the cubic trajectory mentioned by Lenroot et al. [30]. The development of PFC shows continuous and long-term changes throughout the lifespan. The destructive decline in the later period is due to a decrease in brain volume, loss of synapses, and decreased cognitive ability [27]. Many studies have reported that PFC is most sensitive to changes in aging [31], which may be closely related to the function of this area, such as in age-related learning, memory, and other cognitive functions [32, 33].

Hub genes at different stages reflect the development of different functions of PFC

We attempted to elucidate the mechanism driving the evolution of PFC by performing a central analysis in three stages based on evolutionary trends; as a result, we identified several hub genes. Hub genes involved in the evolution of PFC during its fast development phrase are as follows: *STK32B*, *CX3CL1*, *BACH2*, *PCSK1*, *NPPA*, *IPCEF1*, and *RGS4*. Several of these hub genes play specific roles in neuronal differentiation or synapse formation. For example, the gene *STK32B* is upregulated during the fetus period and then enters a suppressed state. This gene encodes a protein involved in synaptic plasticity, learning, memory, and neurodegeneration, and is a key factor in the transmission of information between cells [34]. Therefore, the upregulation of *STK32B* may be related to the development of early cognitive function and synapse formation in PFC. This is not the first time this gene has been found to be expressed in the human cortex [35]. The genes *CX3CL1* and *PCSK1* are involved in the formation of synapses, with *CX3CL1* encoding a chemokine that is highly expressed in dendritic cells [36], which is upregulated after birth and participates in the development of PFC neurons and synapses. The discovery of this gene during PFC development overlaps with the findings of a previous study [13]. The gene *IPCEF1* is expressed in the brain and reported to be involved in nerve injury-induced changes in membrane receptor trafficking [37]. This gene has been repeatedly reported in human brain tissue [38]. In this data analysis, we found that this gene is downregulated in the early stage of PFC development and its expression gradually increases with aging. The gene *RGS4* has been shown to be involved in neuron differentiation and

297 neurite growth [39]. An animal test by Huang et al. [40] showed that *RGS4* deficiency in the
298 prefrontal cortex may be related to schizophrenia-related behaviors. In short, these hub genes play
299 critical roles in the formation of synapses and the development of cognitive functions in the early
300 stage of PFC development.

301 The hub genes involved in the slowing down to a stable period of PFC development are as
302 follows: *EVI2A*, *SLC31A2*, *TF*, and *GJB6*. These genes are related to the conduction of nerve
303 impulses and the electrophysiological balance of cell membranes. The function of the *EVI2A* gene
304 is related to transmembrane signaling receptor activity. Mladinov and colleagues reported that this
305 gene is differentially expressed in the dorsolateral and medial orbitofrontal cortex of patients with
306 schizophrenia [41]. The other three genes are involved in the transmembrane transport of different
307 substances. Among them, the protein encoded by the gene *TF* mediates the transport of iron ions,
308 balances iron levels in the body, and participates in myelination and remyelination of the central
309 nervous system [42]. It has been shown that dysfunction of this gene is related to Parkinson's
310 disease [43]. Finally, *GJB6* is regulated by glucocorticoids in the brain to provide energy and
311 maintain the supply of nutrients to the brain [44, 45].

312 The hub genes involved in the late stage of PFC are as follows: *SLC31A2*, *GJB6*, *PLLP*, and
313 *CLDN10*. The function of the gene *GJB6* has been described above. The gene *PLLP* has been
314 shown to encode myelin structural proteins, and to be involved in the development of myelin
315 around neurons and maintaining the integrity of the myelin structure [46, 47]. Hamacher and
316 colleagues reported the isolation of *PLLP* in mammalian brain, and noted that the mutated product
317 of this gene may be involved in Bardet–Biedl syndrome type 2 (BBS2) [48]. These genes play
318 active roles in maintaining the structural integrity of the nervous system during PFC decline.

319 Most of the genes that are pivotal at different stages of PFC evolution related to brain function
320 development and related diseases, have been evaluated in previous studies; but for some of them
321 there is no clear connection to human brain development. This requires further experimental
322 analysis, although this is beyond the scope of the present study. In summary, our analysis shows
323 that, during the fast development period of PFC, the hub genes mainly regulate the proliferation

and differentiation of neurons and the development of synapses. In the stable period of PFC evolution, the hub genes mainly maintain the stability of PFC in the human brain by maintaining nerve impulses and electrophysiological balance. Finally, during the stage of decline of PFC, the hub genes mainly function to combat the degradation of nerve fibers. This also illustrates the microstructure involved in the evolution of PFC throughout the lifespan.

Pathways regulate PFC evolution through hub genes

The five chosen pathways experience changes along with the evolution of human PFC. Among them, the *Axon guidance pathway* is the most sensitive to aging throughout the lifespan. It is well known that axons are an important component of neurons and play an important role in the development of the human cerebral cortex. During the critical period of human cerebral cortex development, the *Axon guidance pathway* is highly developed. As the number of neurons increases until the PFC develops completely, with aging, the synapses in the frontal lobe begin to be pruned and decline [49], nerve function declines, and synaptic incapacitation occurs. This overlaps with the results of another study describing that synapse-related pathways decline with age [13]. As a pathway directly related to PFC development, this pathway may regulate the development of PFC mainly through the *LRRC4C* and *PARD6G* genes (Fig. 7). The gene *LRRC4C* has been reported to be involved in the regulation of axon development and synaptic development, and its deficit can cause neurodevelopmental disorders [50]. In the case of the gene *PARD6G*, it was found to be involved in synaptic modification [51].

For the *Dopaminergic synapse pathway*, *Platelet activation pathway*, and *FoxO signaling pathway*, we also found literature to support the findings. As a neuromodulator, dopamine (DA) plays a vital role in the normal cognitive processes of PFC [52]. The hub genes *PRKCB* and *GNG7* may play important roles in this pathway. The protein encoded by the *PRKCB* gene is involved in a variety of cellular signaling pathways, and it was found in mouse experiments that this kinase may also be involved in regular neuronal function and endocrine regulation, which are related to emotional response behavior [53]. Regarding the hub gene *GNG7*, it was found to be involved in motor control between dopamine-mediated striatum neurons [54]. The brain is one of the regions

of the body with an abundance of blood. It is thus unsurprising that the *Platelet activation pathway* develops in parallel with PFC. Our analysis showed the roles of the hub genes *TLN2* and *RASGRP2* in linking this pathway with PFC development. The hub gene *TLN2* is thought to be involved in atherosclerosis [55]. The *RASGRP2* gene encodes the main signaling molecule in platelets, and mutations in this gene affect thrombus formation and cause severe bleeding [56]. The forkhead box O (*FOXO*) transcription factor provides protection for nerve cells during oxidative stress [57]. Our analysis revealed that the hub genes *PRKAB2*, *SMAD3*, and *CCNB1* play key roles in the regulation of PFC development in the *FoxO signaling pathway*. The three genes are mainly involved in the positive regulation of AMPK activity [58], signal transduction [59], and cell cycle control [60].

The *Longevity regulated pathway* showed the slowest pattern of change among the five pathways. The hub genes involved in the *Longevity regulated pathway* are *IGF1* and *PRKAB2*. The proteins encoded by these two genes are involved in the caloric restriction (CR) pathway [61] and the positive regulation of AMPK activity [58], establishing the connection between the pathway and PFC development.

A significant advantage of this study is that the time-varying network of genes related to PFC development was reconstructed through the loggle model, and the evolutionary pattern of gene interactions in the PFC region was found at the gene level, rather than simply changes in gene expression. At the same time, at different stages of evolution, genes involved in human cortical development that overlap with those described in previous studies were identified. In addition, the evolution of synaptic and other related pathways in the evolution of PFC was also verified. Although we related genes and pathways to PFC evolution based on the proposed time-varying graphical modeling and analytical procedures, the current study does have some limitations. Owing to the specificity of the tissue site, the current gene level analysis of the human cerebral cortex is almost entirely dependent on the examination of postmortem tissue and the data are not from a cohort study. In addition, we hope to integrate other omics data such as miRNA, DNA

methylation, and proteomics data into the network analysis, to obtain a more comprehensive picture of PFC evolution and development. We plan to pursue these issues in future work.

Methods

Estimating time-varying graphs with the loggle model

This study aims to characterize the evolutionary pattern of inter-gene interactions over time in the human PFC region and identify hub genes involved in evolution. Accordingly, we first used the loggle model [19] to build and understand PFC time-varying network graphs. In particular, compared with several other time-varying graph model construction methods that use fused-lasso-type penalties to estimate the piecewise constant to identify the jump points (e.g., TESLA [63], TVGL [64], GFGL [65]), the loggle model used in this work assumes that the graph topology changes smoothly over time, and uses the local group-lasso-type penalty to reasonably combine the information of adjacent time points to ensure the progressive change of the graph structure. Then, the ADMM algorithm was used to solve the convex optimization problem, and a blockwise fast algorithm and pseudo-likelihood approximation were used to solve the "computational disaster" problem. The PFC time-varying graphs were constructed using the loggle package in R. To make the work self-contained, we here briefly describe how to construct the time-varying network graph via the loggle model. More technical details can be found in the paper by Yang and Peng [19].

Local Group Graphical Lasso Estimation

Suppose $\mathrm{X(t)} = (X^1(\mathrm{t}), X^2(\mathrm{t}), \ldots, X^p(\mathrm{t}))^T$ is a p-dimensional time-series random vector at time $t \in [0, 1]$, which obeys a multivariate Gaussian distribution $\mathcal{N}_p(\mu(t), \sum(t))$. We used $\{x_k\}$ ($k \in \{1, \ldots, \mathrm{N}\}$) to indicate the observation at time $t_k (0 \leq t_1 \leq \ldots \leq t_k \leq \ldots t_N \leq 1)$, where N represents the sample size. For simplicity, we centered the observations x_k by subtracting the estimated mean $\hat{\mu}(t_k)$ from x_k so that each x_k is drawn independently from $\mathcal{N}_p(0, \sum(t))$.

We next estimated the precision matrix $\Omega(t)$ ($\Omega(t) = \Sigma^{-1}(t)$) to construct the graph edge set. The loggle model assumes the smoothness of the graphical topology, that is, the edge set of the graph changes gradually over time. The model obtains the estimated precision matrix $\widehat{\Omega}(t_k)$ at

the *k*th time point by combining the locally weighted negative log-likelihood function with the local group lasso penalty [66]:

$$\mathcal{L}(\Omega_k) \coloneqq \frac{1}{\sqrt{|\mathcal{N}_{k,d}|}}\sum_{i\in\mathcal{N}_{k,d}}\left[tr\left(\Omega(t_i)\hat{\Sigma}(t_i)\right) - \log|\Omega(t_i)|\right] + \lambda\sum_{u\neq v}\sqrt{\sum_{i\in\mathcal{N}_{k,d}}\Omega_{uv}(t_i)^2}, \quad (1)$$

where $\mathcal{N}_{k,d} = \{i \in \mathrm{I} : |t_i - t_k| \leq d\}$ is the time index with the center t_k and neighborhood width *d*; $|\mathcal{N}_{k,d}|$ is the cardinality of $\mathcal{N}_{k,d}$; $\Omega_k = \{\Omega(t_i)\}_{i\in\mathcal{N}_{k,d}}$ is a set of precision matrices with $\Omega_{uv}(t_i)$ representing the (*u, v*)-th element in Ω; $\hat{\Sigma}(t_i) = \sum_{j=1}^{N}\omega_h^{t_j}(t)x_j x_j^T$ is the kernel estimate of the covariance matrix, with $\omega_h^{t_j}(t) = \frac{K_h(t_j - t)}{\sum_{j=1}^{N}K_h(t_j - t)}$ as the weight and $K_h(\cdot) = K(\cdot/h)$ as a symmetric nonnegative kernel function with bandwidth *h*.

Model fitting and optimization

The model uses the alternating directions method of multipliers (ADMM) algorithm [67] to solve the convex optimization problem for objective function (1). Unfortunately, the ADMM algorithm involves eigen-decomposition, which can take a long time when the data dimensionality is large. To solve the "computational disaster" problem, the algorithm introduces a fast blockwise algorithm [68, 69] and a pseudo-likelihood approximation [70, 71] to the objective function.

Specifically, the *p* variables are completely separated into multiple nonoverlapping blocks by the following necessary and sufficient condition after suitable permutation; then, the ADMM algorithm is applied to each block to speed up the computation and reduce the calculation time from $O(p^3)$ to $\sum_{l=1}^{L}O(p_l^3)$. In addition, the pseudo-likelihood approximation can speed up the calculation efficiency by changing the problem of estimating the sparse pattern of the precision matrix to estimating the sparsity pattern of the regression coefficients. Further, the paired group lasso penalty [72] is used to ensure the symmetry of the edge selection.

Parameter adjustment

When learning the loggle model, there are three parameters involved: the kernel bandwidth *h*; the neighborhood width *d*, which controls the smoothness of the graph over time; and the sparsity parameter λ, which controls the degree of graph sparsity. Their tuning parameters are learned by cross-validation (CV) at each time point. For this purpose, data are divided into training and

validation sets. The validation score on the *j*th validation set is defined as:

$$CV_j(t_k;\lambda_k,d_k,h) = tr\left(\hat{\Omega}^{rf}_{-(j)}(t_k;d_k,\lambda_k,h)\hat{\Sigma}_{(j)}(t_k)\right) - \log\left|\hat{\Omega}^{rf}_{-(j)}(t_k;d_k,\lambda_k,h)\right|.$$

The K-fold cross-validation score at time t_k is defined as $\mathrm{CV}(t_k;\lambda_k,d_k,h) = \sum_{j=1}^{K} CV_j\,(t_k;\lambda_k,d_k,h)$. The smallest CV score corresponds to the optimal combination of parameters (h, λ_k, d_k). At the same time, the "majority vote" procedure cv.vote [73] was introduced to effectively reduce the false discovery rate. The algorithm flow involved in the loggle model is shown in Fig. 8.

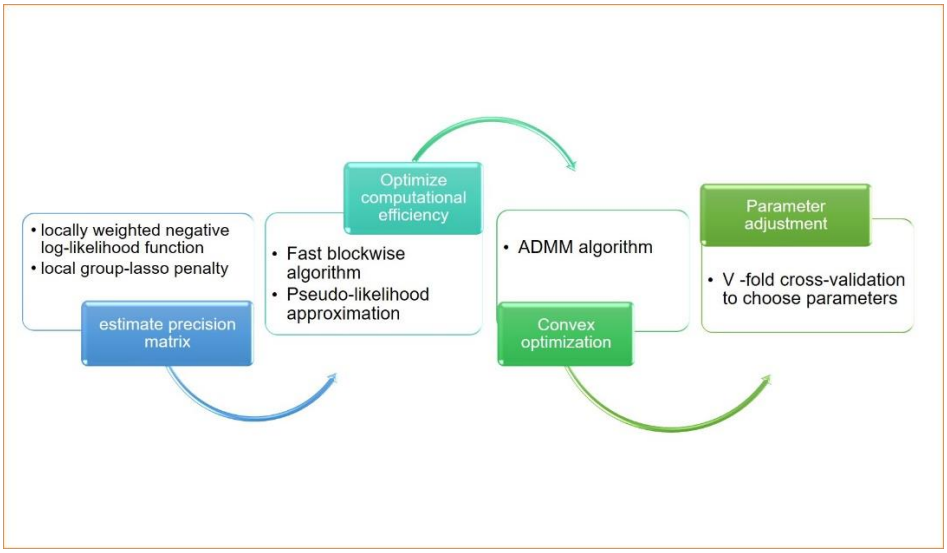


Fig. 8 The main algorithm flow chart involved in the loggle model.

Parameter setting

Given the nine time points, we performed a threefold CV to determine the tuning parameters h, d, and λ of the graph at each time point. In particular, we took one validation set every three time points and treated the remaining data as the training set. For example, the first fold validation set includes time t_1, t_4, t_7, and the rest as the training set. The second fold validation set includes t_2, t_5, t_8, and so on. The loggle model assumes that data measured at different time points are independent, which makes the CV setting in this application valid [19]. The early grid search stop threshold is 8; that is, the grid search stops when the number of edges exceeds $8p$ where p is the number of variables. The threshold for cv.vote is set to 0.8; that is, by fitting the model in each training set, only the edges that appear in at least 80% of these models are retained.

Comparison with other models

We further compared the performance of loggle with two existing special models of loggle, namely, kernel and invar. kernel uses the smoothness of the covariance matrix by introducing a kernel estimate $\hat{\Sigma}(t)$ into the likelihood function [74] and by setting the parameter d=0, but the model ignores the potential smoothness of the graph. invar is performed to estimate $\Omega(t_k)$ by using the global group lasso penalty [75] with d=1; thus, the generated graphs do not change over time.

Global network properties

Observing different network properties can provide valuable insights into the redistribution of genes within biological networks as well as the evolution of biological network structures. We used several common network properties to explain the trend of change of the network topology: number of nodes, number of edges, network *diameter*, network *density*, and *exclusive edges*.

The network *diameter* represents the maximal distance (shortest path) among all of the distances calculated between each pair of nodes in a network [76], that is, $D = \max_{i,j} \delta_{min}(i,j)$, where $\delta_{min}(i,j)$ represents the shortest path between nodes i and j. A "high" network diameter indicates that the compactness between nodes in the network is low. In particular, comparing network diameters at different time points can predict network development in a timely manner [76].

The *network density* shows the sparseness or density of the graph based on the number of connections per node set, and is defined as $d(G)= \frac{2|E|}{|V|(|V|-1)}$. Some researchers asserted that biological networks are usually sparsely connected because this helps to ensure robustness in evolution [77]. The *exclusive edge* metric indicates that some edges belong to a certain network and do not appear in the rest of the network.

Network similarity analysis

Considering that nine different time points will likely generate different networks, we calculated the similarity between networks and merged similar networks into groups. Based on this, we analyzed the evolution of PFC at different stages. This analysis used the *CompNet neighbor similarity index* (CNSI) to measure the similarity between two compared networks. CNSI

measures the similarity of each pair of nodes by comparing the degree of overlap between the first neighbors of the nodes between two networks. A cumulative overall similarity score for all nodes is calculated to specify similarities between two compared networks [78], that is, $CNSI = \sum_{i=1}^{N} \frac{f_{n_i}^A \cap f_{n_i}^B}{f_{n_i}^A \cup f_{n_i}^B}$, where n_i represents the i-th node of the two compared networks, and $f_{n_i}^A$ and $f_{n_i}^B$ refer to the first neighbor of the i-th node in the corresponding two compared networks.

Central analysis

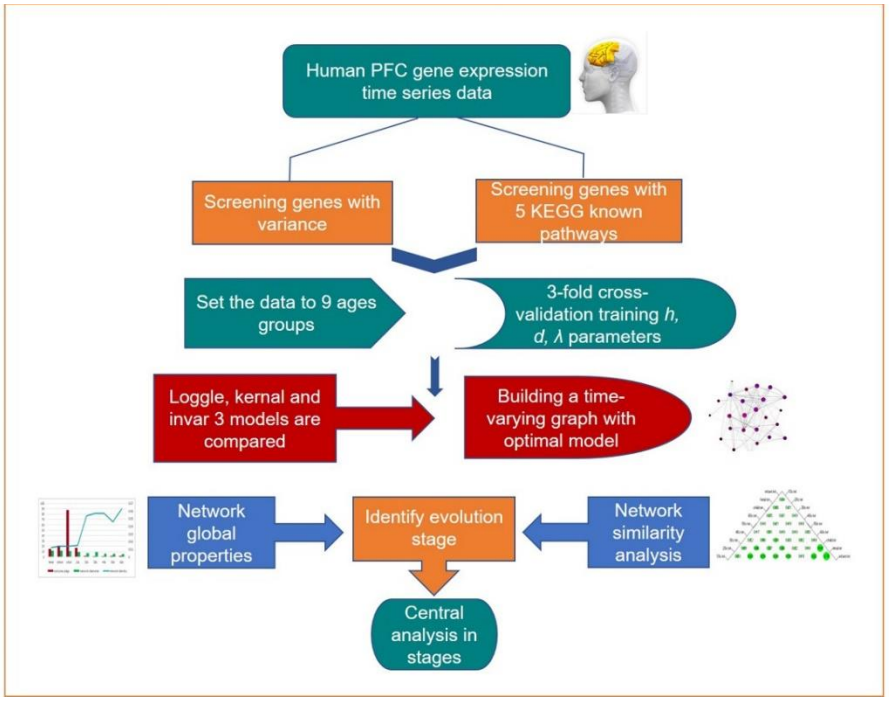


Fig. 9 Detailed procedure for investigating the evolutionary pattern of human PFC gene interaction networks and hub genes

Biological networks are usually scale-free networks with very few high-degree nodes but many low-degree ones. Changes in some important nodes not only affect nodes adjacent to them, but also affect the topology of the entire network [76]. To find important genes in human PFC tissue, we further calculated the *degree* of nodes to perform a central analysis on the constructed network. *Degree*, corresponding to the number of nodes directly connected to a given node *V* (the number of directly connected edges), namely, the first neighbors [76], is expressed as $C_d(i) = deg(i)$. A high-degree node is called a "hub," and removing such a node affects the network topology and

further leads to disturbances in biological systems [79]. The degree calculation was performed in Cytoscape and is displayed with the node size corresponding to its value. Fig. 9 shows a flow chart of the main methods and processes used for exploring the evolution of PFC in this study.

Acknowledgments

We thank Liwen Bianji, Edanz Group China (www.liwenbianji.cn/ac), for editing the English text of a draft of this manuscript.

Supplementary information

Additional file 1. Supplementary Figures and Tables

Additional file 2. Gene network edges-List at different age periods

Abbreviations

PFC (Prefrontal cortex); Loggle (Local Group Graphical Lasso Estimation); KEGG (Kyoto Encyclopedia of Genes and Genomes); GEO (Gene Expression Omnibus); Bardet-Biedl syndrome type 2 (BBS2); forkhead box O (FOXO); caloric restriction (CR); CompNet neighbor similarity index (CNSI); cross-validation (CV)

Author's contributions

HW performed the analysis and wrote the manuscript. YW, JS, ZL participated in data analysis and interpretation. HC and YC conceptualized the idea and revised the manuscript. All authors read and approved the final manuscript.

Funding

National Natural Science Foundation of China (71403156 to HC); Shanxi Scholarship Council of China (2017-054 to HC); Applied Basic Research Program of Shanxi Province (201901D111204 to HC); and a fund from Michigan State University (to YC).

Availability of data and materials

The gene expression data that support the findings of this study are available in GEO database (http://www.ncbi.nlm.nih.gov/geo) with the Gene Expression Omnibus accession number GSE30272. All data generated and results analyzed during this study are included in this article

and its supplementary information.

Ethics approval and consent to participate

Not applicable.

Competing interests

The authors declare that they have no competing interests.

Author details

[1]Division of Health Statistics, School of Public Health, Shanxi Medical University, Taiyuan, Shanxi 030001, PR China. [2]School of Sport and Physical Education, North University of China, Taiyuan, Shanxi 030051, PR China. [3]Department of Statistics and Probability, Michigan State University, East Lansing, MI 48824, USA

References

1. Fuster, J.N.M.. The prefrontal cortex—An update: Time is of the essence. Neuron, 2001. **30**(2): p. 319-333.
2. Hathaway, W.R. and B.W. Newton. Neuroanatomy, Prefrontal Cortex, in StatPearls. 2019, StatPearls Publishing StatPearls Publishing LLC.: Treasure Island (FL).
3. Fellows, L.K.. Advances in understanding ventromedial prefrontal function: the accountant joins the executive. Neurology, 2007. **68**(13): p. 991-995.
4. Fuster, J.. Anatomy of the Prefrontal Cortex. John Libbey Eurotext, 2003. p. 1-10.
5. Jaffe A E , Shin J , Collado-Torres L , et al. Developmental regulation of human cortex transcription and its clinical relevance at single base resolution. Nature Neuroscience, 2014. **18**(1): p. 154-161.
6. Shaw P , Kabani N J , Lerch J P , et al. Neurodevelopmental trajectories of the human cerebral cortex. Journal of Neuroscience, 2008. **28**(14): p. 3586-3594.
7. Molnár Z, Clowry G J , Šestan N, et al. New insights into the development of the human cerebral cortex. Journal of anatomy, 2019.
8. Case, R.. The role of the frontal lobes in the regulation of cognitive development. Brain Cogn, 1992. **20**(1): p. 51-73.
9. Anderson V A , Anderson P , Northam E , et al. Development of executive functions through late childhood and adolescence in an Australian sample. Developmental Neuropsychology, 2001. **20**(1): p. 385-406.
10. Diamond, A. and B. Doar. The performance of human infants on a measure of frontal cortex function, the delayed response task. Developmental Psychobiology, 1989. **22**(3): p. 271-294.
11. Luciana, M. and C.A. Nelson. The functional emergence of prefrontally-guided working memory systems in four- to eight-year-old children. Neuropsychologia, 1998. **36**(3): p. 273-293.
12. Kolb B , Mychasiuk R , Muhammad A , et al. Experience and the developing prefrontal cortex.

Proceedings of the National Academy of Sciences of the United States of America. **109**(Supplement_2): p. 17186-17193.
13. Wruck, W. and J. Adjaye. Meta-analysis of human prefrontal cortex reveals activation of GFAP and decline of synaptic transmission in the aging brain. Acta Neuropathologica Communications, 2020. **8**(1): p. 26.
14. Liu X , Somel M , Tang L , et al. Extension of cortical synaptic development distinguishes humans from chimpanzees and macaques. Genome Res, 2012. **22**(4): p. 611-622.
15. Moreau M P , Bruse S E , Jornsten R , et al. Chronological changes in microRNA expression in the developing human brain. PloS one, 2013. **8**(4): p. e60480-e60480.
16. Wang, W. and G.Z. Wang. Understanding Molecular Mechanisms of the Brain Through Transcriptomics. Front Physiol, 2019. **10**: p. 214.
17. Chandrasekaran, S. and D. Bonchev. Network analysis of human post-mortem microarrays reveals novel genes, microRNAs, and mechanistic scenarios of potential importance in fighting huntington's disease. Comput Struct Biotechnol J, 2016. **14**: p. 117-130.
18. Zhang, W.F., C.C. Liu, and H. Yan. Clustering of temporal gene expression data by regularized spline regression and an energy based similarity measure. Pattern Recognition, 2010. **43**(12): p. 3969-3976.
19. Yang, J. and J. Peng. Estimating Time-Varying Graphical Models. Journal of Computational and Graphical Statistics, 2018 **29:1,** 191-202
20. Drton, M. and M. Perlman. Model selection for Gaussian concentration graphs. Biometrika, 2004. **91**(3): p. 591-602.
21. Gibberd, A.J. and J.D.B. Nelson. Regularized Estimation of Piecewise Constant Gaussian Graphical Models: The Group-Fused Graphical Lasso. Statistics, 2015(3): p. 1-12.
22. Le, S., K. Mladen, and E.P. Xing. KELLER: estimating time-varying interactions between genes. Bioinformatics, 2009. **25**(12): p. 128-36.
23. Kolar, M. and E.P. Xing. Estimating Networks With Jumps. Electronic Journal of Statistics, 2013. **6**(1): p. 2069-2106.
24. Gibberd, A.J. and J.D.B. Nelson. High dimensional changepoint detection with a dynamic graphical lasso. in IEEE International Conference on Acoustics. 2014.
25. Fuster, J.M.. Frontal lobe and cognitive development. Journal of Neurocytology, 2002. **31**(3-5): p. 373-385.
26. Teffer, K. and K. Semendeferi. Human prefrontal cortex: evolution, development, and pathology. Prog Brain Res, 2012. **195**: p. 191-218.
27. Salthouse, T.A.. When does age-related cognitive decline begin? Neurobiology of Aging, 2009. **30**(4): p. 507-514.
28. Anderson V A, Anderson P, Northam E, et al. Development of Executive Functions Through Late Childhood and Adolescence in an Australian Sample. Developmental neuropsychology, 2001. **20**: p. 385-406.
29. Masliah E , Mallory M , Hansen L A , et al. Quantitative synaptic alterations in the human neocortex during normal aging. Neurology, 1993. **43**(1): p. 192-197.
30. Lenroot, R.K. and J.N. Giedd. Brain development in children and adolescents: insights from anatomical magnetic resonance imaging. Neurosci Biobehav Rev, 2006. **30**(6): p. 718-729.

31. Jernigan T L , Archibald S L , Fennema-Notestine C , et al. Effects of age on tissues and regions of the cerebrum and cerebellum. Neurobiology of Aging, 2001. **22**(4): p. 581-594.
32. Salat, D. and J. Kaye, Js. Prefrontal gray and white matter volumes in healthy aging and Alzheimer disease. Archives of Neurology, 1999. **56**(3): p. 338.
33. Veluw S J, Sawyer E K, Clover L, et al. Prefrontal cortex cytoarchitecture in normal aging and Alzheimer's disease: a relationship with IQ. Brain Structure & Function, 2012. **217**(4): p. 797-808.
34. Temtamy S A , Aglan M S , Valencia M , et al. Long interspersed nuclear element-1 (LINE1)-mediated deletion ofEVC,EVC2,C4orf6, andSTK32B in Ellis–van Creveld syndrome with borderline intelligence. Human mutation, 2008. **29**: p. 931-938.
35. Ciuculete, D.M., Boström, A.E., Tuunainen, A.K., et al. Changes in methylation within the STK32B promoter are associated with an increased risk for generalized anxiety disorder in adolescents. Journal of Psychiatric Research, 2018. **102**: p. 44-51.
36. Gunner, G., Cheadle, L., Johnson, K.M. et al. Sensory lesioning induces microglial synapse elimination via ADAM10 and fractalkine signaling. 2019. **22**(7): p. 1075-1088.
37. Guan, X., X. Zhu, and Y.X. Tao, Peripheral nerve injury up-regulates expression of interactor protein for cytohesin exchange factor 1 (IPCEF1) mRNA in rat dorsal root ganglion. Naunyn Schmiedebergs Arch Pharmacol, 2009. **380**(5): p. 459-63.
38. Sunkin S M , Lydia N , Chris L , et al. Allen Brain Atlas: an integrated spatio-temporal portal for exploring the central nervous system. Nucleic Acids Research, 2012. **41**(D1): p. D996-D1008.
39. Pallaki P , Georganta E M , Serafimidis I , et al. A novel regulatory role of RGS4 in STAT5B activation, neurite outgrowth and neuronal differentiation. Neuropharmacology, 2017. **117**: p. 408-421.
40. Huang, M.W., et al., RGS4 deficit in prefrontal cortex contributes to the behaviors related to schizophrenia via system xc(-)-mediated glutamatergic dysfunction in mice. Theranostics, 2018. **8**(17): p. 4781-4794.
41. Mladinov, M., et al., Gene expression profiling of the dorsolateral and medial orbitofrontal cortex in schizophrenia. Translational Neuroscience, 2016. **7**(1): p. 139-150.
42. Tomás R. Carden, Correale J , Pasquini J M , et al. Transferrin Enhances Microglial Phagocytic Capacity. Mol Neurobiol, 2019. **56**(9): p. 6324-6340.
43. Qian-Qian S , Yong-Sheng Y , Yan Z , et al. Plasma transferrin level correlates with the tremor-dominant phenotype of Parkinson's disease. Neurosci Lett, 2018. **684**: p. 42-46.
44. Yuting L , Ruili Z , Zhenying W , et al. Mechanistic effect of the human GJB6 gene and its mutations in HaCaT cell proliferation and apoptosis. Brazilian journal of medical and biological research = Revista brasileira de pesquisas medicas e biologicas, 2018. **51**(9): p. e7560-e7560.
45. Juszczak, G.R. and A.M. Stankiewicz. Glucocorticoids, genes and brain function. Prog Neuropsychopharmacol Biol Psychiatry, 2018. **82**: p. 136-168.
46. Fischer, I. and V.S. Sapirstein. Molecular cloning of plasmolipin. Characterization of a novel proteolipid restricted to brain and kidney. J Biol Chem, 1994. **269**(40): p. 24912-9.
47. Yaffe Y , Hugger I , Yassaf I N , et al. The myelin proteolipid plasmolipin forms oligomers and induces liquid-ordered membranes in the Golgi complex. J Cell Sci, 2015. **128**(13): p. 2293-302.
48. Hamacher M , Pippirs U , Angelika Köhler, et al. Plasmolipin: genomic structure, chromosomal localization, protein expression pattern, and putative association with Bardet-Biedl syndrome. Mamm

Genome, 2001. **12**(12): p. 933-7.
49. Masliah E , Mallory M , Hansen L A , et al. Quantitative synaptic alterations in the human neocortex during normal aging. Neurology, 1993. **43**(1): p. 192-197.
50. Maussion G , Cruceanu C , Rosenfeld J A , et al. Implication of LRRC4C and DPP6 in neurodevelopmental disorders. American Journal of Medical Genetics Part A, 2016. **173**(2): p. 395.
51. Marques E , Englund J I , Tervonen T A , et al. Par6G suppresses cell proliferation and is targeted by loss-of-function mutations in multiple cancers. Oncogene, 2016. **35**(11): p. 1386-98.
52. Seamans, J.K. and C.R. Yang. The principal features and mechanisms of dopamine modulation in the prefrontal cortex. Prog Neurobiol, 2004. **74**(1): p. 1-58.
53. Hayashi T , Shibata H , Kurihara I , et al. High Glucose Stimulates Mineralocorticoid Receptor Transcriptional Activity Through the Protein Kinase C β Signaling. International Heart Journal, 2017. 58(5):794.
54. Sasaki, Keita, Yamasaki, Tatsuro, Omotuyi, Idowu O, et al. Age-dependent dystonia in striatal Gγ7 deficient mice is reversed by the dopamine D2 receptor agonist pramipexole. Journal of Neurochemistry. **124**(6): p. 844-854.
55. von Essen, Magdaléna, Rahikainen R , Oksala N , et al. Talin and vinculin are downregulated in atherosclerotic plaque; Tampere Vascular Study. Atherosclerosis, 2016. **255**: p. 43-53.
56. Matthias, C., et al., Human CalDAG-GEFI gene (RASGRP2) mutation affects platelet function and causes severe bleeding. Journal of Experimental Medicine, 2014. **211**(7): p. 1349.
57. Maiese, K., Z.Z. Chong, and Y.C. Shang. "Sly as a FOXO": new paths with Forkhead signaling in the brain. Curr Neurovasc Res, 2007. **4**(4): p. 295-302.
58. Nagy, S., G.W. Maurer, and J.L. Hentze. AMPK signaling linked to the schizophrenia-associated 1q21.1 deletion is required for neuronal and sleep maintenance. 2018. **14**(12): p. e1007623.
59. Ma X , Das N K , Castillo C , et al. SMAD family member 3 (SMAD3) and SMAD4 repress HIF2alpha-dependent iron-regulatory genes. J Biol Chem, 2019. **294**(11): p. 3974-3986.
60. Fang Y , Yu H , Liang X , et al. Chk1-induced CCNB1 overexpression promotes cell proliferation and tumor growth in human colorectal cancer. Cancer Biology & Therapy. **15**(9): p. 1268-1279.
61. Barzilai N , Huffman D M , Muzumdar R H , et al. The critical role of metabolic pathways in aging. Diabetes, 2012. **61**(6): p. 1315-22.
62. Colantuoni C , Lipska B K , Ye T , et al. Temporal dynamics and genetic control of transcription in the human prefrontal cortex. Nature, 2011. **478**(7370): p. 519-23.
63. Ahmed, A. and E.P. Xing. Recovering time-varying networks of dependencies in social and biological studies. Proc Natl Acad Sci U S A, 2009. **106**(29): p. 11878-83.
64. Hallac D , Park Y , Boyd S , et al. Network Inference via the Time-Varying Graphical Lasso. KDD '17: Proceedings of the 23rd ACM SIGKDD International Conference on Knowledge Discovery and Data Mining, 2017.
65. Gibberd, A.J. and J.D.B. Nelson. Regularized Estimation of Piecewise Constant Gaussian Graphical Models: The Group-Fused Graphical Lasso. Journal of Computational and Graphical Statistics, 2017. **26**(3): p. 623-634.
66. Ming, Y. and L. Yi. Model Selection and Estimation in Regression with Grouped Variables. Journal of the Royal Statistical Society, 2006. **68**(1): p. 49-67.

67. Boyd S , Parikh N , Chu E , et al. Distributed Optimization and Statistical Learning via the Alternating Direction Method of Multipliers. Distributed Optimization and Statistical Learning via the Alternating Direction Method of Multipliers. 2011: now. 1.
68. Witten and M. Daniela. New Insights and Faster Computations for the Graphical Lasso. Journal of Computational & Graphical Statistics, 2011. **20**(4): p. 892-900.
69. Danaher, P., P. Wang, and D.M. Witten. The joint graphical lasso for inverse covariance estimation across multiple classes. Journal of the Royal Statistical Society, 2014. **76**(2): p. 373-397.
70. Meinshausen, N. and P. Bühlmann. High-Dimensional Graphs and Variable Selection with the Lasso. Annals of Statistics, 2006. **34**(3): p. 1436-1462.
71. Ji, and Zhu. Partial Correlation Estimation by Joint Sparse Regression Models. Journal of the American Statistical Association, 2009. **104**(486): p. 735-746.
72. Friedman, J., T. Hastie, and R. Tibshirani. Applications of the Lasso and grouped Lasso to the estimation of sparse graphical models. 2010.
73. Peng J , Zhu J , Bergamaschi A , et al. Regularized multivariate regression for identifying master predictors with application to integrative genomics study of breast cancer. Annals of Applied Statistics, 2009. 4(1): p. 53-77.
74. Zhou, S., J. Lafferty, and L. Wasserman. Time varying undirected graphs. Machine Learning, 2010. **80**(2-3): p. 295-319.
75. Wang, J. and M. Kolar. Inference for Sparse Conditional Precision Matrices. Statistics, 2014.
76. Scardoni, G. and C. Laudanna. Centralities Based Analysis of Complex Networks. New Frontiers in Graph Theory. InTech, 2012.
77. Leclerc, R.D.. Survival of the sparsest: robust gene networks are parsimonious. Mol Syst Biol, 2008. **4**: p. 213.
78. Kuntal, B.K., A. Dutta, and S.S. Mande. CompNet: a GUI based tool for comparison of multiple biological interaction networks. Bmc Bioinformatics, 2016. **17**(1): p. 185.
79. Pavlopoulos G A , Secrier M , Moschopoulos C N , et al. Using graph theory to analyze biological networks. BioData Mining,4,1(2011-04-28), 2011. **4**(1): p. 1-27.

Figures

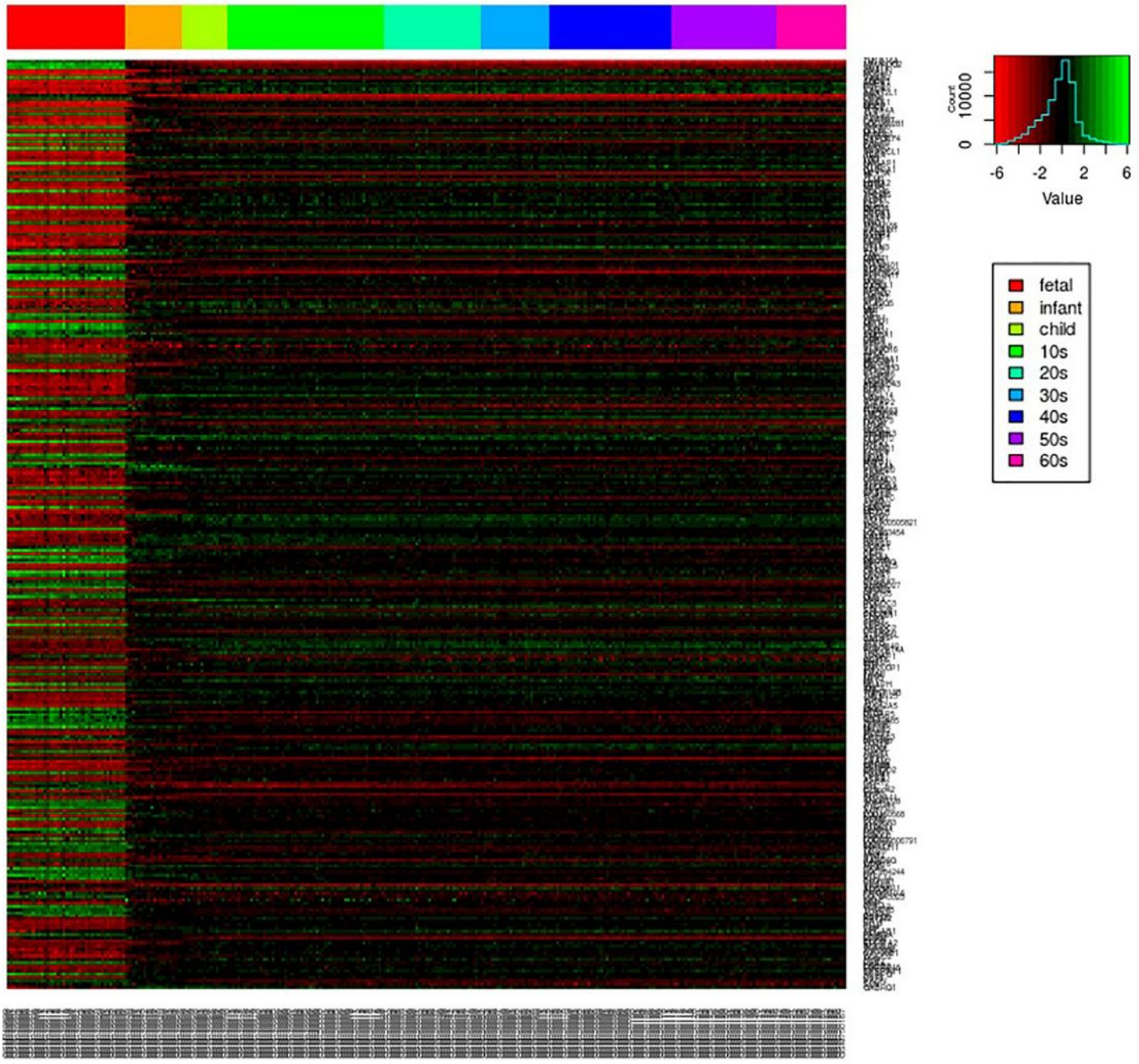


Figure 1

PFC global gene expression changes over time. Each row of the heatmap represents a gene, and each column represents a sample. Each small grid represents the expression of a gene in the sample, with red

representing relatively low expression and green high expression. Different colored bars at the top of the graph indicate the age group to which the sample belongs, as shown in the legend on the right.

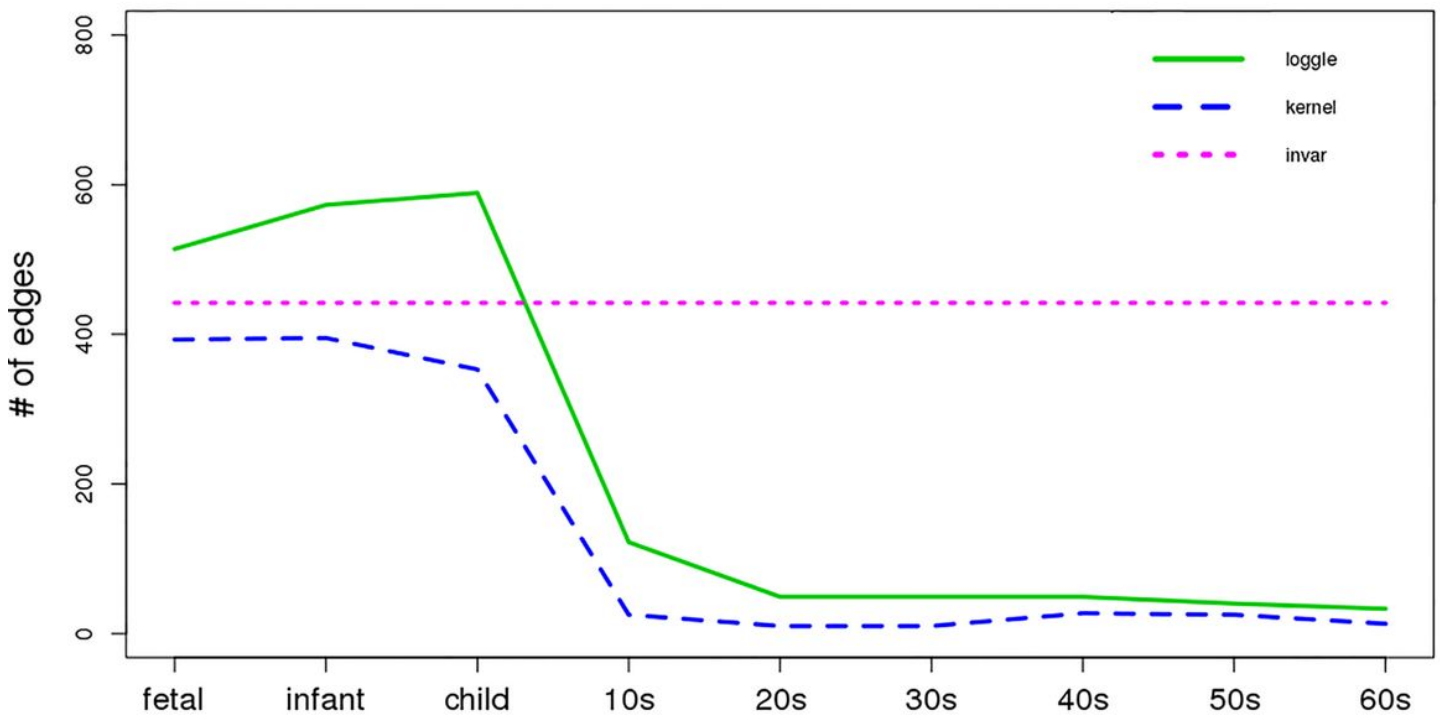


Figure 2

Number of edges vs. age period (x-axis). Different line types represent different models.

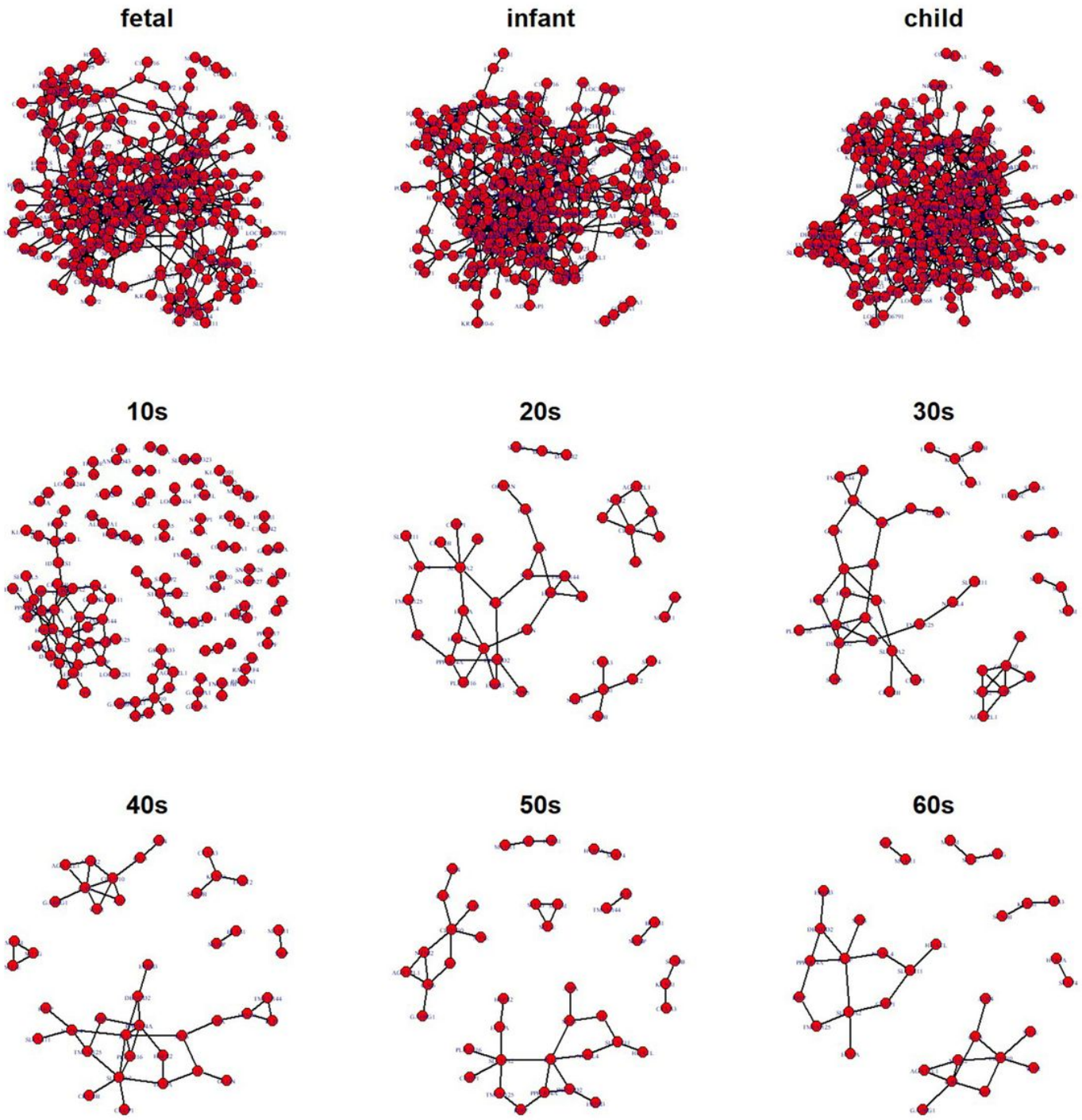


Figure 3

Display of networks corresponding to the nine age periods. Nodes represent genes and connections between nodes indicate interactions between genes.

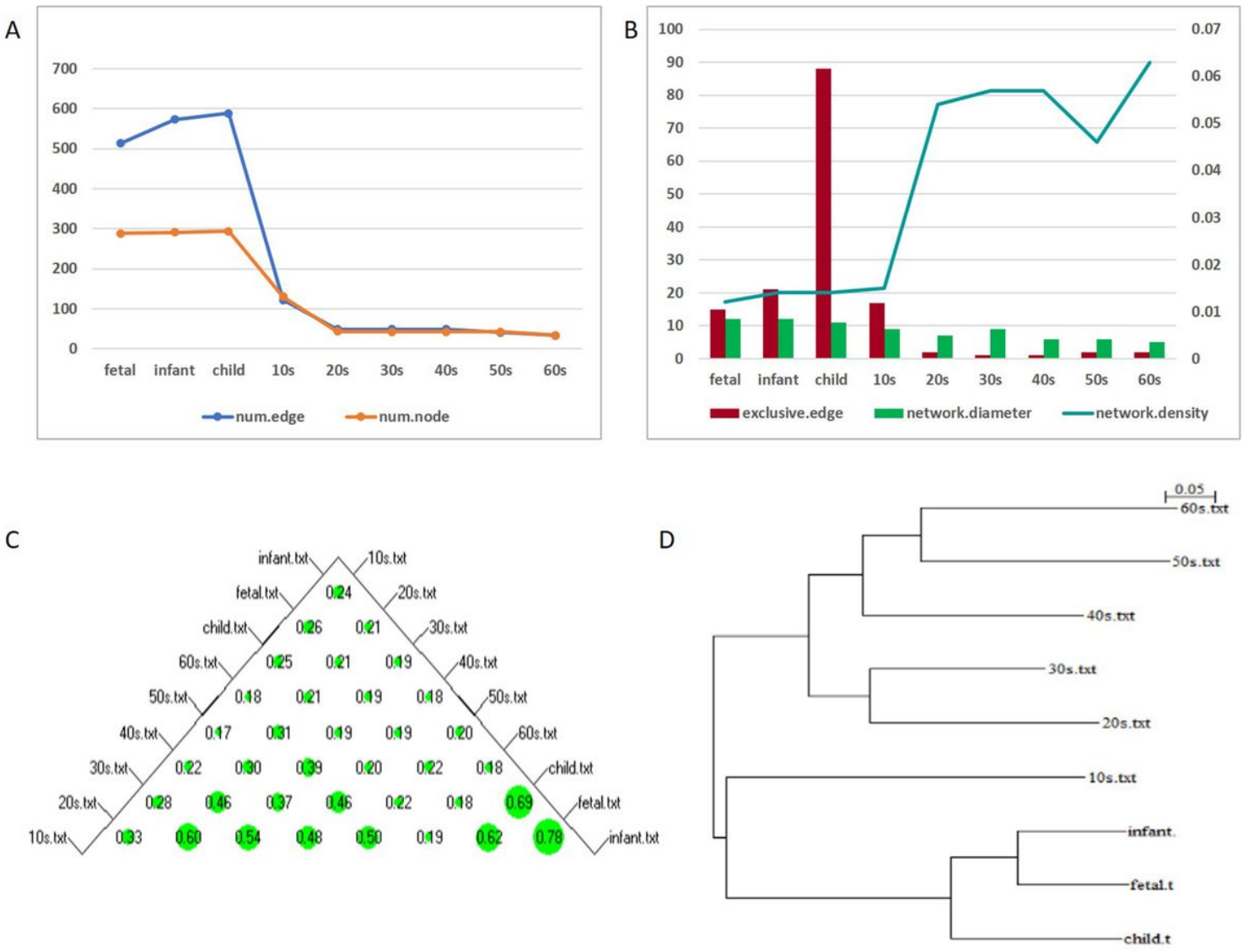


Figure 4

Network topology change. (A) shows the numbers of edges and nodes included in the network at different ages. (B) represents the specific edge (left y-axis), network diameter (left y-axis), and network density (right y-axis) in the network corresponding to each age period. (C) shows a bubble chart of a similarity matrix generated based on the CNSI. Larger bubbles indicate higher similarity of the corresponding two networks. (D) is a hierarchical clustering tree dendrogram generated based on the similarity matrix.

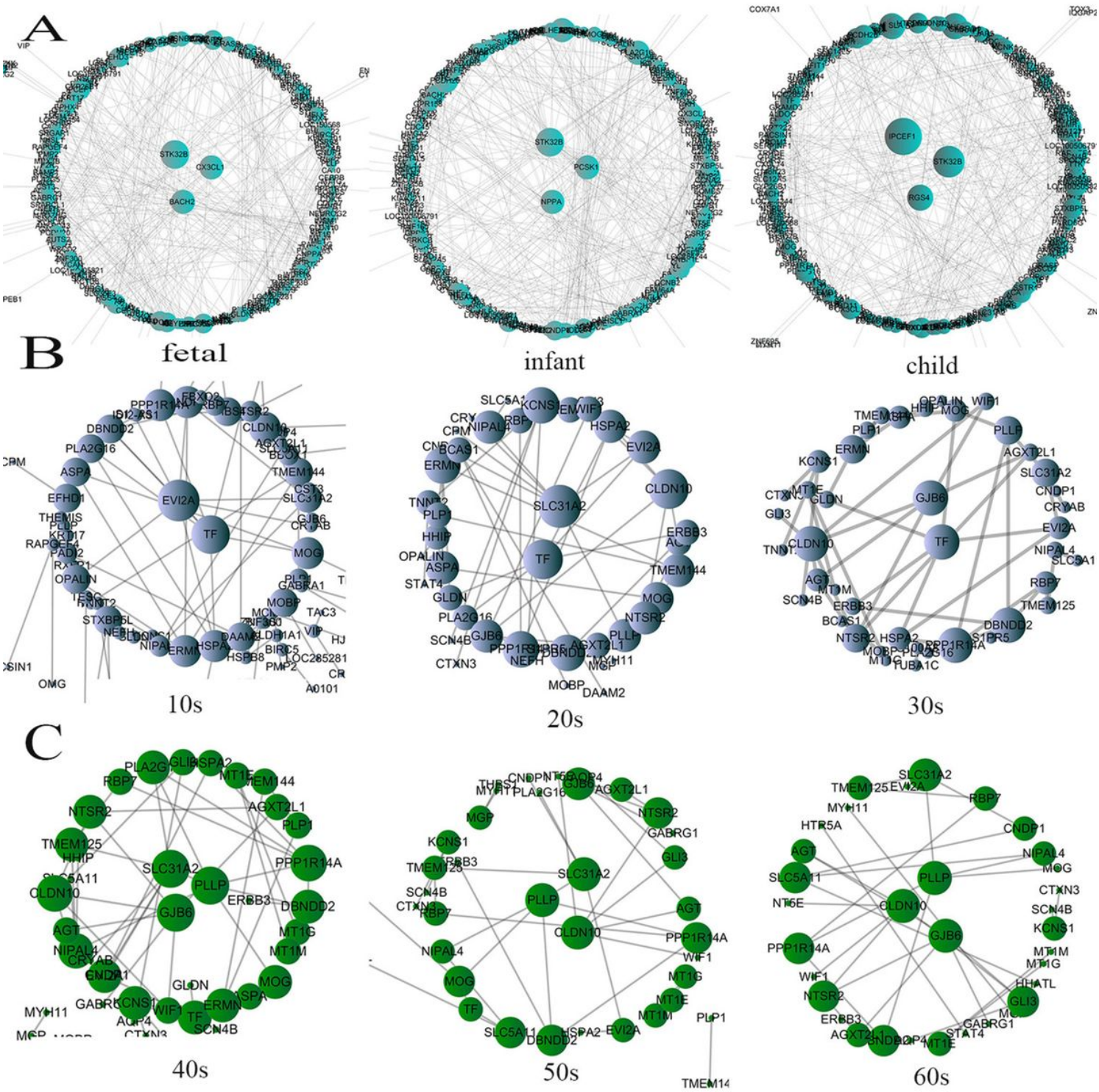


Figure 5

Identification of hub genes throughout the lifespan in PFC evolution. (A) shows the fast development period of PFC evolution, namely, fetus, infant, and child; (B) shows that the evolution of PFC gradually declined to a stable period, that is, 10s, 20s, and 30s; (C) demonstrates the destructive recession period in PFC evolution, namely, 40s, 50s, and 60s. A larger node size in the graph corresponds to a higher node degree. Nodes with the highest degree are considered to be hubs and are placed in the network center.

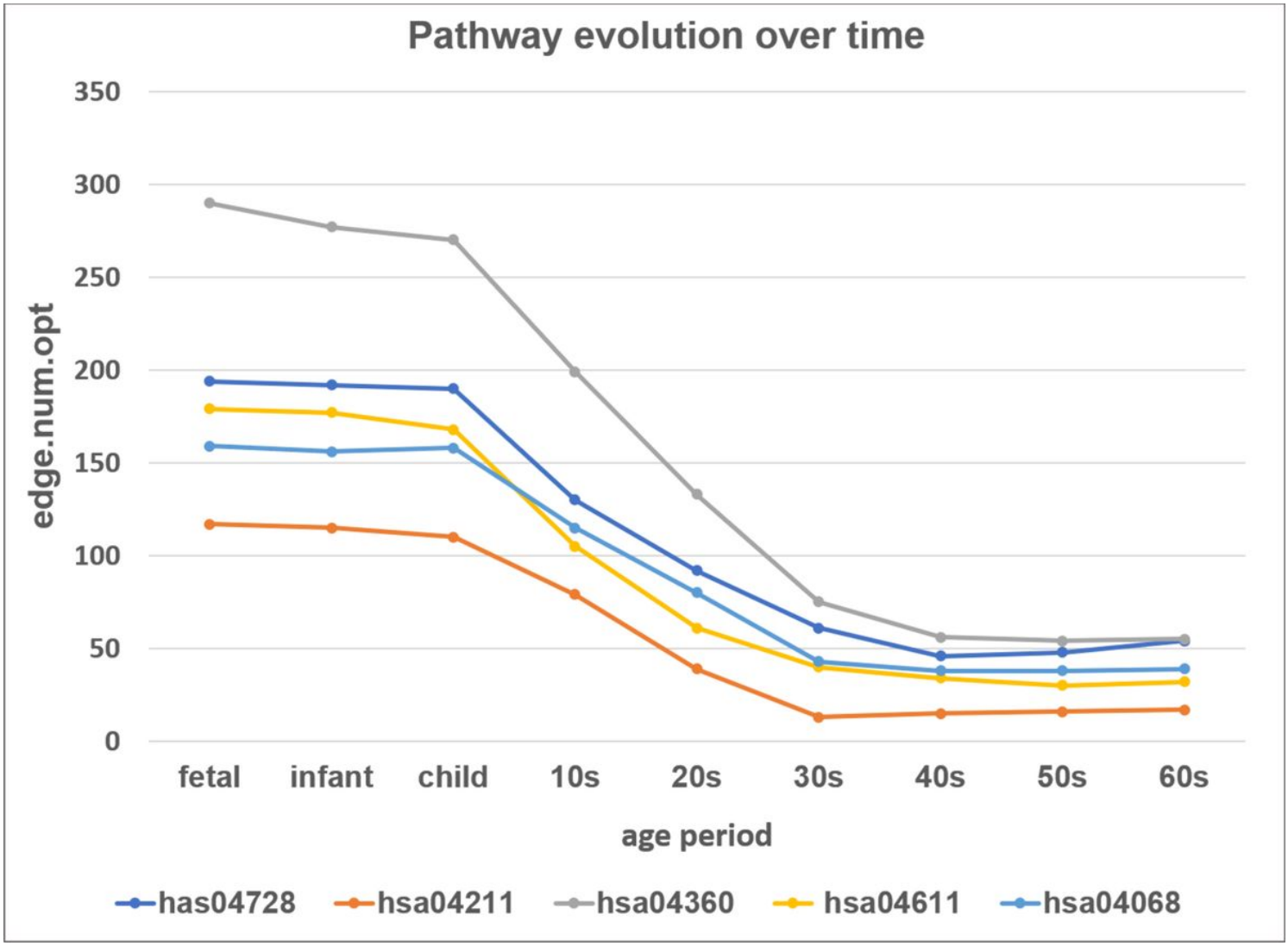


Figure 6

The evolution of the time-varying networks over different age periods. The y-axis shows the optimal number of edges at each developmental stage.

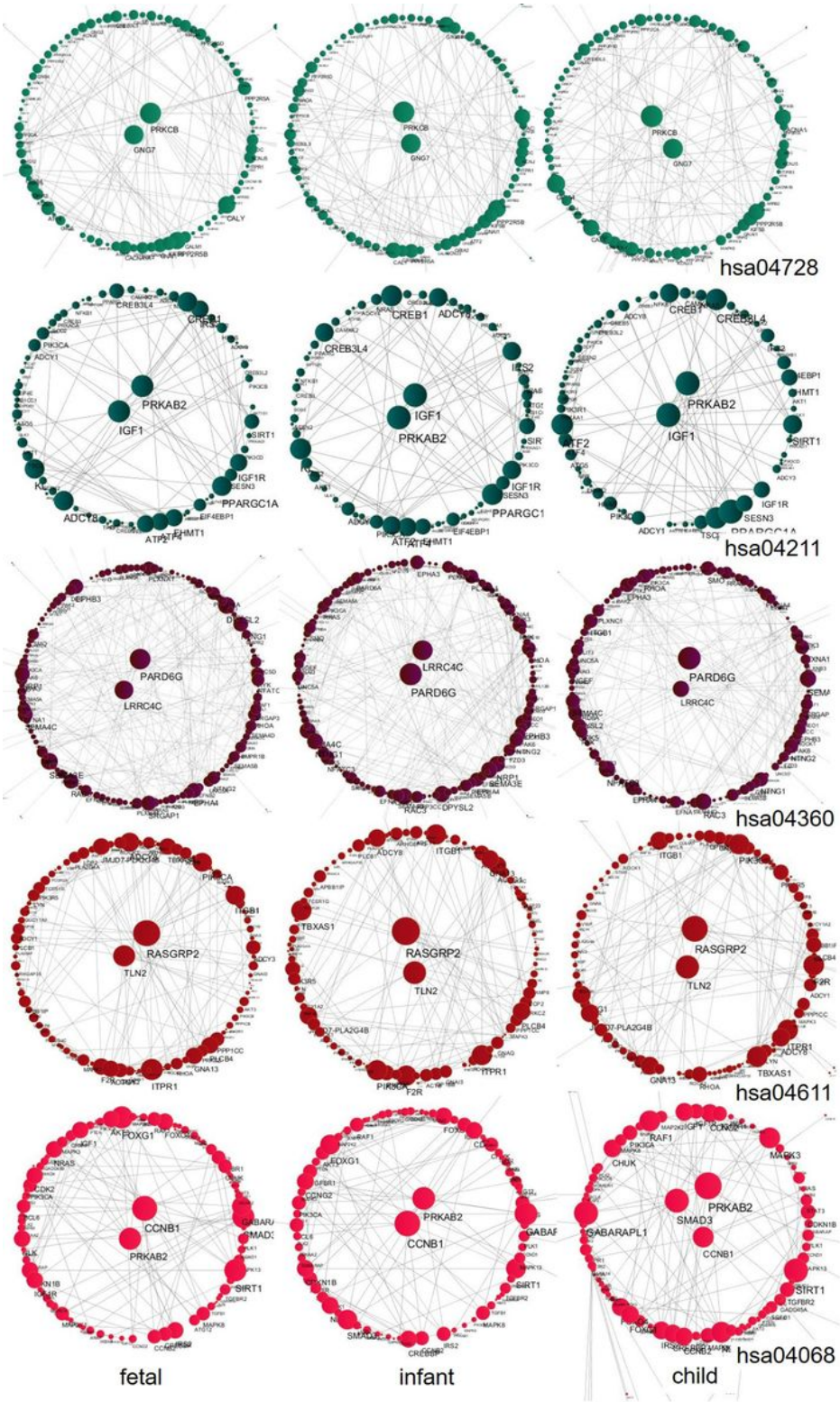


Figure 7

Central analysis of networks corresponding to the fast development stage (fetus, infant, and child) for the five pathways. A larger node corresponds to a larger node degree. Hub genes with large node degree values in each network are placed in the center of the network.

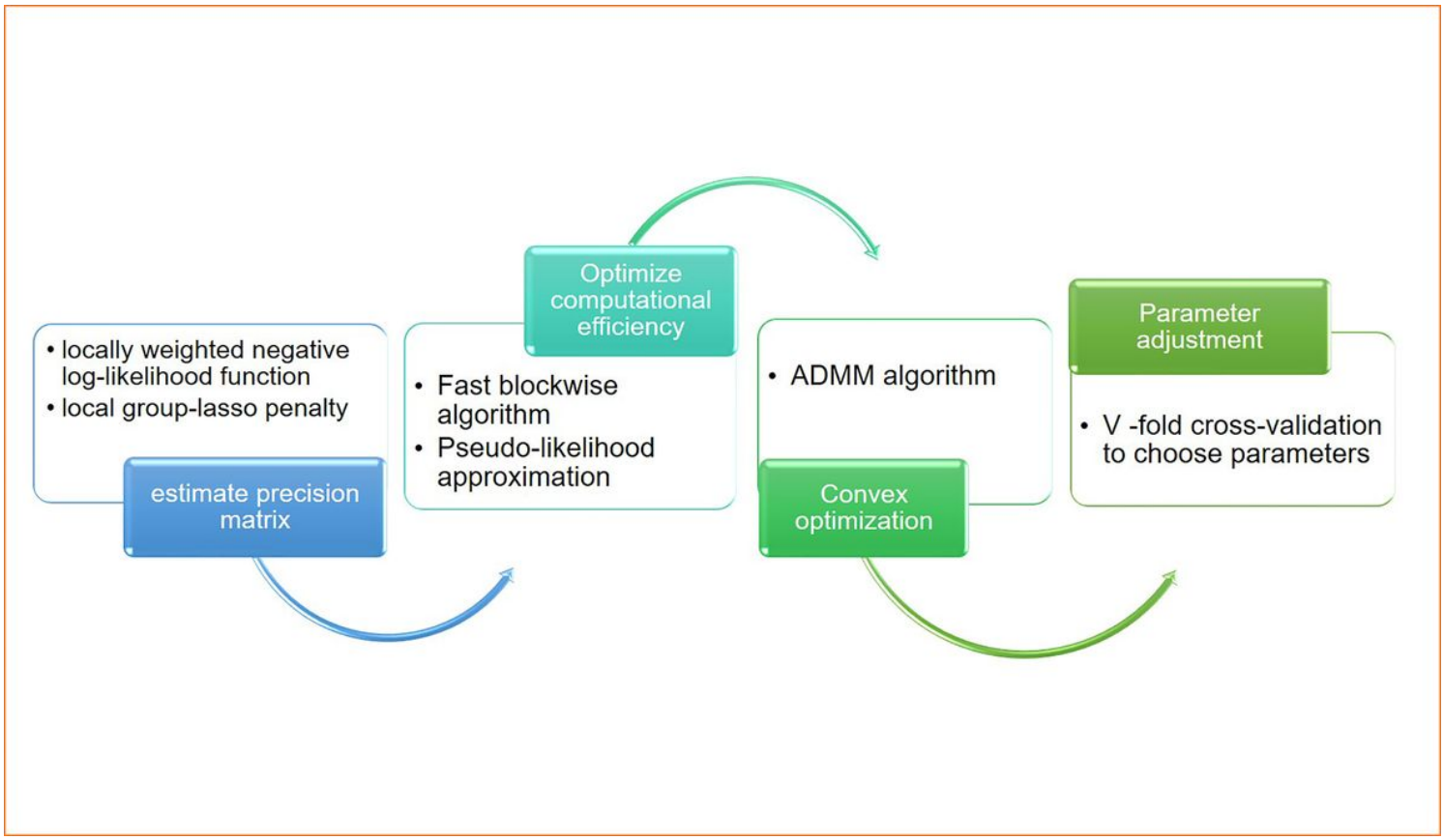


Figure 8

The main algorithm flow chart involved in the loggle model.

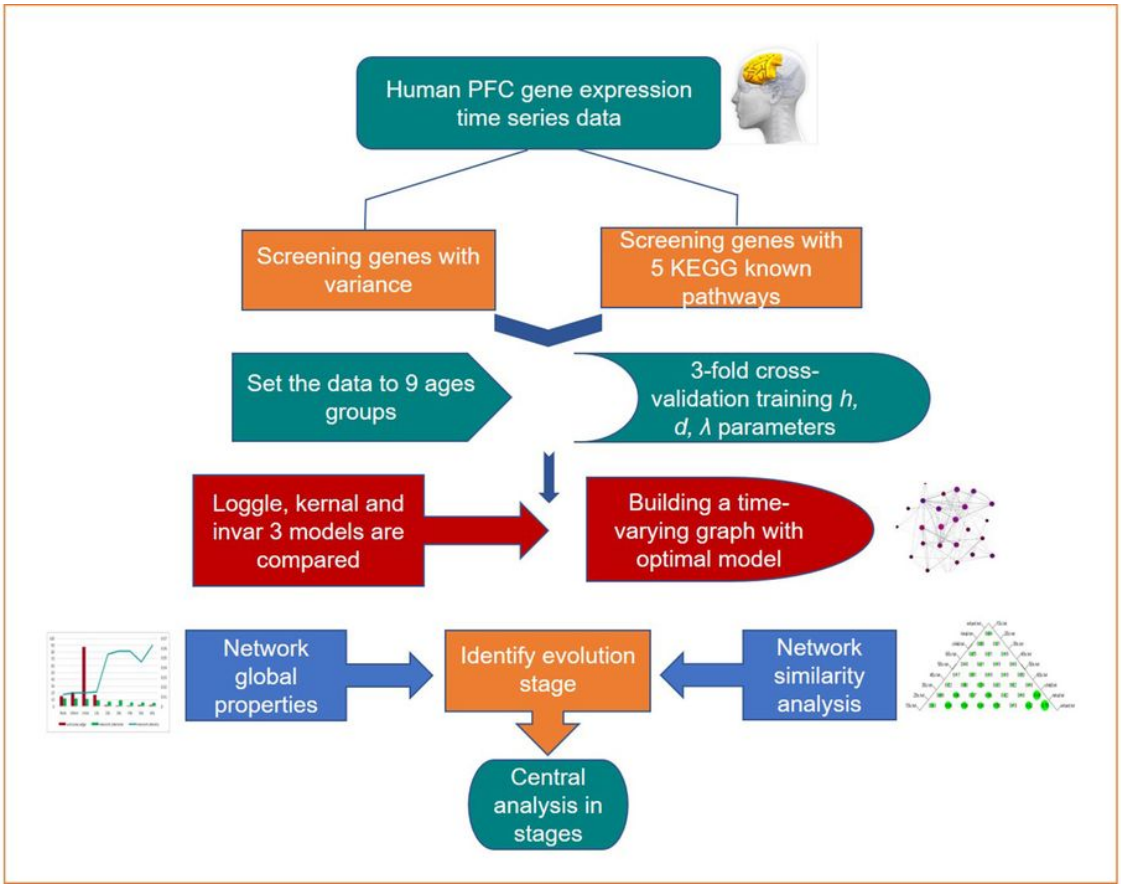


Figure 9

Detailed procedure for investigating the evolutionary pattern of human PFC gene interaction networks and hub genes

Supplementary Files

This is a list of supplementary files associated with this preprint. Click to download.

- Supplementalfile2Listofnetworkedges.xlsx
- Supplementalfile1.pdf